4 [^{111}In-DTPA^{0}-D-Phe^{1}]-Octreotide: The Ligand—The Receptor—The Label

Antonios Zanglis

4.1 The Somatostatin Peptide Family

Almost half a century ago, in the first January 1973 issue of *Science*, the Roger Guillemin group in the Salk Institute (La Jolla, California), published a paper that proved the presence of a bioactive peptide in ovine hypothalamic extracts, with inhibitory effect in the secretion of immunoreactive growth hormone (GH). In the same paper, the structure of this 14-peptide was elucidated and its synthetic form was shown to elicit the same biological response in rats and humans, as well, hence its name: Somatostatin (SST) or Somatotropin-release inhibiting factor" (SRIF) [1]. SST belongs to the homonymous peptide family with cortistatin (CST). CST-17 is the bioactive cleavage product of a CST precursor peptide in humans, being a relatively recent addition. CST-17 shares common structural and functional features with SST (SST: SST-14 and SST-28 are the bioactive peptides, see Fig. 4.1), such as the depression of neuronal activity and some distinct properties as well, such as the activation of cation selective currents, not responsive to SST. It should be emphasized though, that these peptides (SST and CST) are the products of separate genes [3–5].

A. Zanglis (✉)
National Health System, Athens, Greece

SST is a phylogenetically ancient peptide that is widely distributed throughout the human body. Besides hypothalamus, SST is secreted by various cell populations interspersed mainly in the central and peripheral nervous system, the gut, and the thyroid, although smaller amounts are synthesized by tumor, inflammatory and immune cells (i.e. lymphocytes or macrophages) upon activation. In the gut, SST is produced in the **δ** cells encountered either in the submucous/myenteric plexus or in the pancreatic islets, next to other peptide-producing cell populations (i.e. insulin, glucagon, VIP: vasointestinal peptide), while in the thyroid, SST is localized in a subpopulation of calcitonin-secreting cells (C cells). The gastrointestinal tract is the main source for the assayed SST in plasma (picomolar amounts), taking into consideration its rapid proteolytic degradation in the circulation ($t_{1/2}$ = 1–2 min). The SST-28 and SST-14 peptides with the GH inhibitory activity, start as part of a larger precursor protein (prepro-somatostatin or prepro-SST), the product of the corresponding gene located at the chromosome 3q28 in humans and consists of 116 amino acid residues. Proteolytic cleavage of prepro-SST yields initially pro-somatostatin (contains 92 amino acids), whose further processing at its C-terminal segment yields SST-28 and SST-14 (see Fig. 4.2). The relative amount of these peptides is a tissue- and species-dependent process [7, 8].

G. S. Limouris (ed.), *Liver Intra-arterial PRRT with ^{111}In-Octreotide*,
https://doi.org/10.1007/978-3-030-70773-6_4

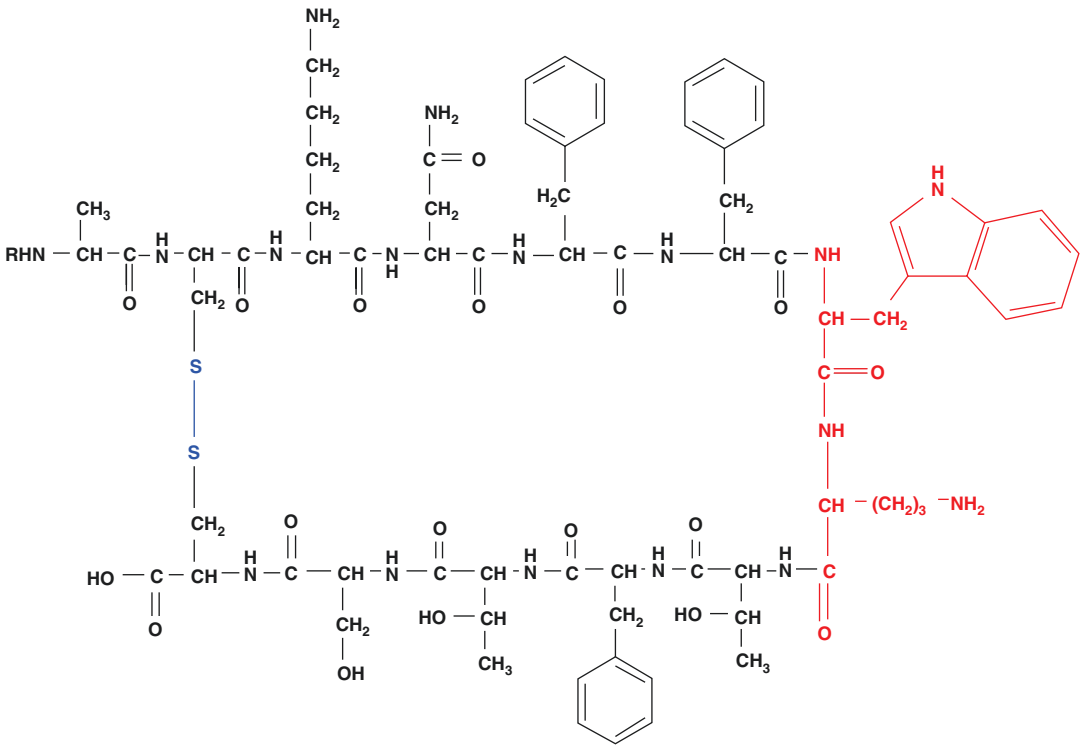

Fig. 4.1 Structure of the natural somatostatin (SST) peptide agonists SST-14 and SST-28. SST-14: R = H and SST-28: R = Ser-Ala-Asn-Ser-Asn-Pro-Ala-Met-Ala-pro-Arg-Glu-Arg-Lys. The pharmacophore (tryptophan and lysine) is highlighted in red [2]

The SST synthesis and release can be stimulated by a variety of hormones, neuropeptides, growth factors, neurotransmitters, cytokines, and nutrients (i.e. GHRH: growth hormone-releasing hormone, neurotensin and CRH: corticotropin-releasing hormone), while other mediators, such as **γ**-aminobutyric acid (GABA) and opiates generally inhibit SST secretion. In this context, the inflammatory cytokines IL-1, TNF-**α,** and IL-6 stimulate and TGF-**β** and leptin inhibit SST synthesis and release. SST acts on various tissues in an autocrine, paracrine, or endocrine fashion [9–11].

The very short biological half-life of somatostatin in the bloodstream, resulting from its vulnerability to the serum peptidases, makes the native bioactive somatostatin molecule (SST-14 or SST-28) unsuitable for imaging or therapy (including radiotherapy) applications. For this reason, the research focused on synthesis of various analogues is devoid of this drawback. The starting point of these efforts was based on the amino acid sequence of the SST-14 molecule and it was soon realized that the central segment of the polypeptide chain (**-Phe^{7}-Trp^{8}-Lys^{9}-Thr^{10}-**) was responsible for the SSTR binding. The main modification of a shortened portion (octapeptide) of the original SST-14 molecule was the substitution of certain key L-amino acids by their D-counterparts (i.e. L-Phe → D-Phe and L-Trp → D-Trp) to render the analogue resistant to the circulating peptidases. In addition, modification of amino acid side chains by incorporation of lipophilic groups (i.e. a 2-naphtalenyl group in place of the methyl group in D-Ala) significantly extended the biological half-life of the synthesized analogues (lanreotide, see Fig. 4.3) and altered its main excretion route (liver vs kidney). The presence of the **-S-S-** bridge between the two cysteine residues is indispensable, since it confers the essential conformational

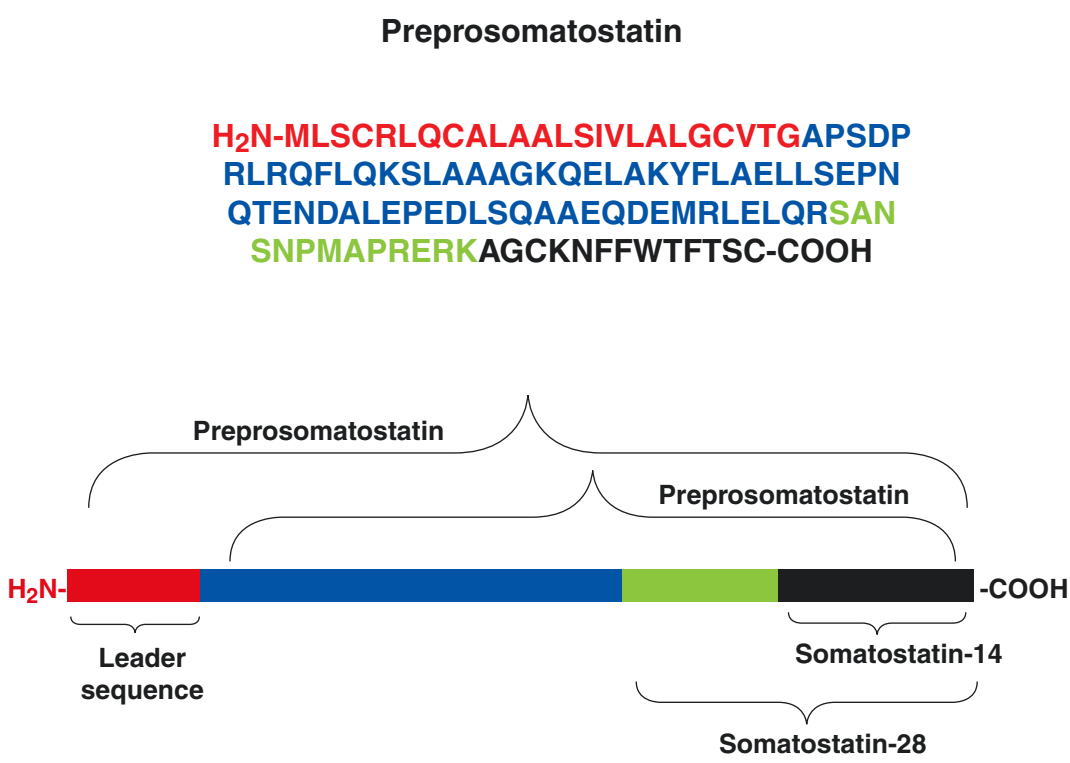

Fig. 4.2 The amino acid sequences of the preprosomatostatin, pre-somatostatin (biologically inactive), somatostatin-28, and somatostatin-14 (biologically active) peptides (one-letter notation [6]). The biologically active sequences reside in the C-end of the precursor molecule [7]

rigidity to the synthesized peptide analogues, in order to maintain their bioactivity. In Fig. 4.3 the structures of some somatostatin analogues (agonists) are drawn. The peptidomimetic JR-11 is the most potent antagonist known so far [9–14].

4.2 The Somatostatin Receptor Family (SSTRs)

4.2.1 Definitions

Agonists are compounds that activate receptors to produce a characteristic set of biological effects.

Full agonists are compounds that act at receptors to effectively trigger the same signal transduction machinery and regulatory pathways as the native ligand.

Partial agonists are compounds that are less effective than full agonists at producing the downstream signaling and regulatory actions by a receptor.

Biased agonists are compounds that effectively elicit only a subset of multiple actions of a receptor for signaling or for receptor regulation**.**

Antagonists bind to receptors but do not activate them and hence are characterized by their ability to block agonist binding and action at a receptor. One needs to distinguish between **neutral antagonists**, which have no activity on their own but will block the effects of an agonist, as opposed to **inverse agonists**, which will inhibit receptor activity in the absence of an agonist, if the receptor exhibits constitutive activity. ***A neutral antagonist does not distinguish between the active or inactive state of the receptor, whereas an inverse agonist prefers the inactive state.***

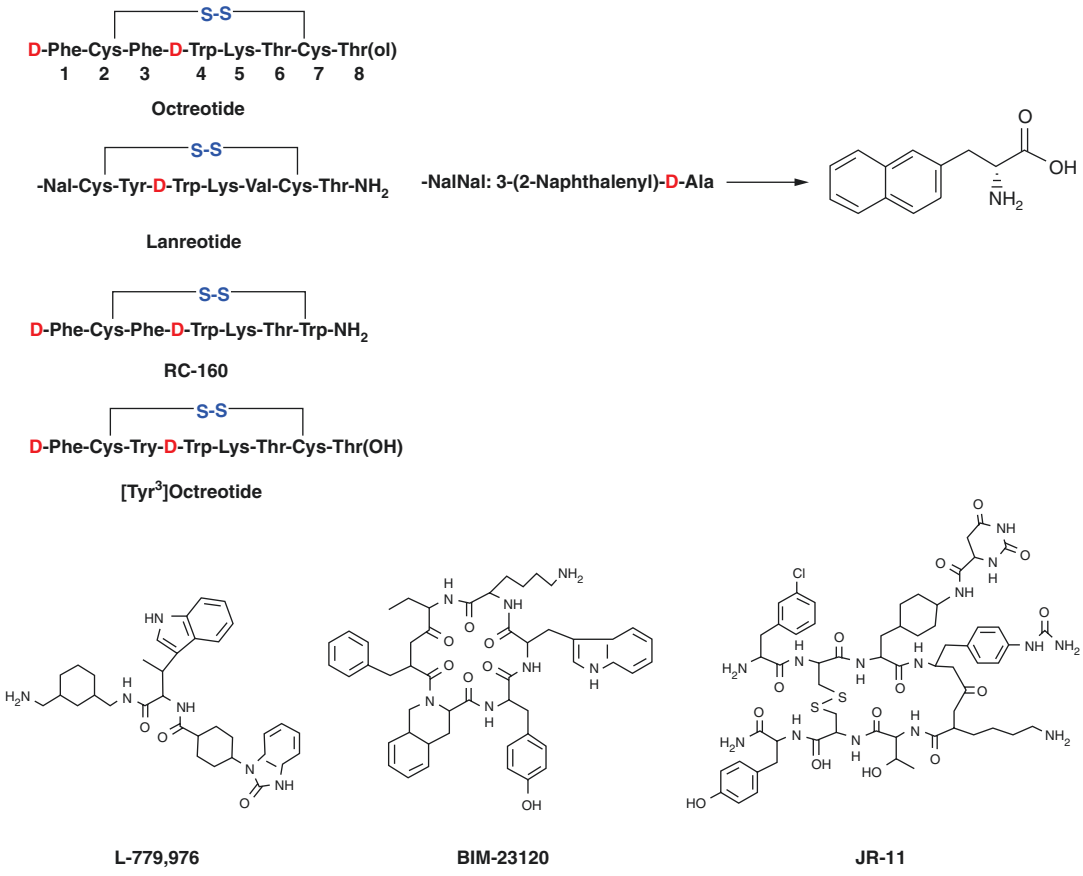

Fig. 4.3 Structures of selected somatostatin analogues (agonists) and antagonists (L-779,976-BIM-2310-JR-11). The presence of D amino acids, the modification of the –COOH end of the molecule (amidation or reduction), and the insertion of a lipophilic group (i.e. 2-naphtalenyl group in lanreotide) have a dramatic impact on the binding of these derivatives by the SSTRs, their solubility, serum half-life, etc. JR-11: Cpa-cyclo[D-Cys-Aph(Hor)-D-Aph(Cbm)-Lys-Thr-Cys]-D-Tyr-NH_2 (Cpa: 4-Cl-phenylalanine, Aph(Hor): 4-amino-L-hydroorotyl-phenylalanine, D-Aph(Cbm): D-4-amino-carbamoyl-phenylalanine

Although somatostatin receptor agonists, biased agonists, and neutral antagonists are known, no somatostatin receptor inverse agonists have been described [11]**.**

4.2.2 Somatostatin Receptors: Biological Function

SST is known to exert a broad range of inhibitory behavior in endocrine (i.e. growth hormone, gastrin, insulin) and exocrine (pancreas) secretory processes, by exerting inhibitory neuromodulatory activity acting as neurotransmitter in central and peripheral nervous system, with antiproliferative and proapoptotic behavior in various tissues [15]. These effects are mediated by the initial binding of SST in G-protein coupled receptors (GPCRs) located at the cell surface of the target cells. The somatostatin receptors (SSTRs) constitute a family of six distinct molecules ($SSTR_1$, $SSTR_{2a}$, $SSTR_{2b}$, $SSTR_3$, $SSTR_4$ and $SSTR_5$), originating from five separate genes. $SSTR_{2a}$ and $SSTR_{2b}$ are alternative splicing variants of the same gene and exhibit a somewhat different tissue distribution ($SSTR_{2a}$ is the prevailing subtype and it is expressed in almost 90% of the various tumors). All SSTSRs are anchored on the cell membrane through seven **α**-helical transmembrane domains and they are widely distributed in

the CNS and peripheral tissues (pancreas, small intestine, etc.). SSTR expression is modulated by various factors, such as thyroid hormones or estrogens, which operate at the transcriptional level [13, 16–19].

There are four known endocytosis mechanisms: macropinocytosis, clathrin-dependent endocytosis, caveola-mediated endocytosis, and caveola/clathrin-independent endocytosis. The SST binding to the SSTRs induces receptor internalization (exception: $SSTR_1$) and/or uncoupling of the receptor from the G-proteins, thus resulting in receptor desensitization, a typical behavior encountered across the GCPR receptor spectrum. These processes appear to be dependent on molecular mechanisms implying selective phosphorylation of the SST-SSTRs (ligand-activated receptors) by G protein–coupled receptor kinases (GRKs) [18–23]. The phosphorylated SSTRs attract the cytoplasmic **β**-arrestins (thus terminating the G protein-mediated cellular response), which promote the endocytosis of the **β**-arrestin-bound receptors by binding to the clathrin-coated pits with the collaboration of adaptors such as adaptor protein AP-2 (see Fig. 4.4). The agonist-induced internalization ability of SSTRs, after binding SST or other analogues, is the key for providing the pathway for the intracellular localization of the various radiolabeled SST-analogues. It is exactly this property that makes the SSTR-targeted radiotherapy with SST-analogues labeled with Auger emitters possible. The affinity of a selected subset of somatostatin analogues (IC_{50}) for the SSTR subtypes is shown in Table 4.1. From this table it becomes evident that even small structural changes in the ligands result in large variations in the SSTR affinity profiles. These structural changes include the binding of

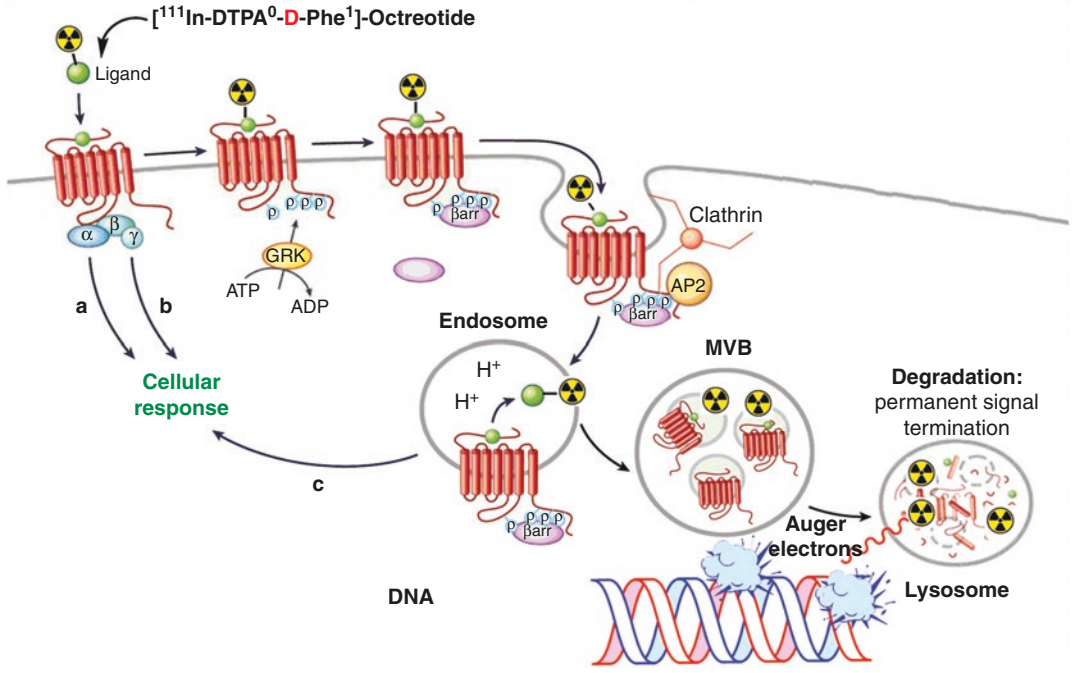

Fig. 4.4 Outline of the receptor-mediated [111In-DTPA0-D-Phe1]-Octreotide internalization process, through clathrin-coated pit and endosome formation and finally lysosomal degradation. SSTR phosphorylation promotes the recruitment of β-arrestins from the cytoplasm, preventing subsequent activation of G proteins by receptors and promoting receptor endocytosis via clathrin-coated pits. The receptors are recycled on the cell-surface (resensitization), while the 111In-labeled degradation products are trapped in the cell and the emitted Auger electrons in the vicinity of the nucleus are highly radiotoxic (modified from [24]). βarr: β-arrestin, AP2 (adaptor complex): A heterotetramer consisting of two large adaptins (alpha and beta), a medium adaptin (mu) and a small adaptin (sigma), GRK: G protein–coupled receptor kinases, MVB: multivesicular body

Table 4.1 Affinity profiles (IC_{50}, nM) for human SSTRs (1–5 subtypes) of selected SST analogues (agonists) [25]

Peptide	$SSTR_1$	$SSTR_2$	$SSTR_3$	$SSTR_4$	$SSTR_5$
SST-28	5.2 ± 0.3	2.7 ± 0.3	7.7 ± 0.9	5.6 ± 0.4	4.0 ± 0.3
Octreotide	>10,000	2.0 ± 0.7	187 ± 55	>1000	22 ± 6
[$DTPA^0$-D-Phe^1]-Octreotide	>10,000	12 ± 2	376 ± 84	>1000	299 ± 50
[^{111}In-$DTPA^0$-D-Phe^1]-Octreotide	>10,000	22 ± 3.6	182 ± 13	>1000	237 ± 52
[$DOTA^0$-D-Phe^1-Tyr^3]-Octreotide	>10,000	14 ± 2.6	880 ± 324	>1000	393 ± 84
[$DTPA^0$-D-Phe^1-Tyr^3]-Octreotate	>10,000	3.9 ± 1	>10,000	>1000	>1000
[^{111}In-$DTPA^0$-D-Phe^1-Tyr^3]-Octreotate	>10,000	1.3 ± 0.2	>10,000	433 ± 16	>1000
[$DOTA^0$-D-Phe^1-Tyr^3]-Octreotate	>10,000	1.5 ± 0.4	>1000	453 ± 176	547 ± 160

the label (In-111) in the case of [^{111}In-$DTPA^0$-D-Phe^1]-Octreotide, the type of the aminocarboxylate chelator (DOTA vs. DTPA), a single aminoacid residue substitution ($Phe^3 \rightarrow Tyr^3$) or changing the charge of the molecule (Octreotate: carries the –COOH group of threonine residue in the C-terminal of the peptide; Octreotide: reduction of the –COOH group of threonine to $–CH_2OH$) [26]. It is interesting to note from Table 4.1 that no analogue exhibits $SSTR_1$ binding affinity [11, 16, 20, 26, 27].

The SSTR subtypes do not appear to internalize somatostatin or somatostatin analogues with the same efficiency and at the same rate. From an in vitro model based on Chinese hamster ovary (CHO)-K_1 cells, stably expressing one of the five human SSTRs subtypes ($SSTR_2$, $SSTR_3$, $SSTR_4$ and $SSTR_5$), a rapid (within minutes) agonist-dependent internalization of a ^{125}I-labeled SST-28 ligand in a time- and temperature-dependent manner was observed. The maximum of the radioligand internalization was observed 60 min later. In this model, the $SSTR_3$ and $SSTR_5$ expressing cells exhibited the highest degree of internalization (78% and 66%, respectively), followed by $SSTR_4$ (29%) and $SSTR_2$ (20%), while the $SSTR_1$ subtype expressing cells displayed only a negligible amount of internalization (4%). The degree of internalization of the SSTR-ligand complex, besides being the receptor subtype-dependent, has been demonstrated to be ligand-dependent as well. For example, the [^{111}In-$DTPA^0$-D-Phe^1-Tyr^3]-Octreotate analogue exhibits the highest degree of internalization from the analogues of Table 4.1, an observation that has been confirmed in vivo in rats and humans [2, 14, 16, 18–20, 28].

Besides normal tissues, SSTRs are found on the cell surface of various tumor cells, such as tumors of pituitary, pancreatic, breast, and hematopoietic origin including their metastases. In general, $SSTR_{2a}$ is the most common SSTR subtype found in human tumors, followed by $SSTR_1$, with $SSTR_3$ and $SSTR_4$ being far less common. $SSTR_5$ appears to be more tumor specific with strong expression in some tumors (i.e. breast) and complete absence in others (i.e. pancreatic). The high density and frequency of SSTR expression in human tumors has been widely exploited as a therapeutic target and for imaging. It should be noted that more than one type of SSTRs may be expressed by the same tumor. Table 4.2 summarizes the various tumor types and their respective SSTR expression pattern, which inevitably leads to the wide variations observed in the % uptake of the labeled somatostatin analogues used in imaging or therapy of these neoplasms [19].

A fairly recent development in the field of SSTR targeting was the introduction of SSTR antagonists, which seemed to recognize more receptor binding sites on the cell surface. SSTR antagonists showed favorable pharmacokinetics and better tumor visualization than agonists, despite their very poor internalization rates (internalization is the sine qua non for radiotherapeutic applications of somatostatin analogues labeled with Auger-emitting isotopes). The binding of the SSTR antagonists has been found to be always higher compared to that of somatostatin analogues (agonists) in experiments with human tumor specimens, and this remarkable result can be easily appreciated from the data in Table 4.3. The somatostatin antagonist JR-11 is so far the most potent and selective among the available

Table 4.2 Variation in the expression pattern of SSTR subtypes in some human tumors. Data are based on mRNA, RT-PCR, Northern blotting, and in situ hybridization studies. The values in parentheses indicate the total number of tumors studied [22]. *GEP* Gastroenteropancreatic, *ICT* Islet Cell Tumor, *MCT* Medullary Thyroid Carcinoma

	SSTR subtype									
	$SSTR_1$		$SSTR_2$		$SSTR_3$		$SSTR_4$		$SSTR_5$	
Tumor	mRNA	Protein	mRNA	Protein	mRNA	Protein	mRNA	Protein	mRNA	Protein
Pituitary tumor										
Somatotroph	44% (25)		96% (28)		44% (25)		5% (22)		86% (22)	
Lactotroph	84% (19)		63% (19)		35% 17)		6% (17)		71% (17)	
Nonfunctioning	38% (24)		75% (24)		43% (23)		13% (23)		485 (23)	
Corticotroph	56% (9)		67% (9)		25% (8)		0% (7)		86% (7)	
Neuroendocrine GEP tumors										
Carcinoid	76% (59)	88% (8)	80% (84)	78% (63)	43% (58)		68% (47)		77% (44)	
Gastrinoma	79% (28)	100% (5)	93% (28)	100% (8)	36% (28)		61% (23)		93% (28)	
Insulinoma	76% (21)		81% (21)		38% (21)		58% (19)		57% (21)	
Nonfunctioning ICT	58% (24)		88% (24)		42% (24)		48% (21)		50% (24)	
Renal Ca	85% (13)		100% (13)		0% (13)		50% (12)			
Breast Ca	33% (103)	52% (33)	99% (103)	48% (33)	38% (101)	48% (33)	23% (97)		18% (51)	
Meningioma	46% (24)		100% (24)		33% (24)		50% (12)		71% (14)	
Glioma	100% (7)		100% (7)		67% (6)		71% (7)		57% (7)	
Neuroblastoma	0% (6)		100% (15)		17% (6)					
Colorectal Ca	27% (41)		87% (41)		22% (41)		10% (41)		46% (41)	
MTC	29% (14)		79% (14)		36% (14)		0% (14)		64% (14)	
Pheochromocytoma	100% (11)	80% (5)	100% (11)	90% (20)	73% (11)		73% (11)		73% (11)	

Table 4.3 The extent of the binding in selected tumors expressing $SSTR_2$ of an agonist (^{125}I-Tyr^3-Octreotide vs. an antagonist (^{125}I-JR-11). The superiority of the antagonist binding is obvious [14, 21]. Data are mean ± SEM

Tumor	Samples (*n*)	Antagonist ^{125}I-JR-11 binding (dpm/mg)	Agonist ^{125}I-Tyr^3-Octreotide binding (dpm/mg)	Agonist/ Antagonist ratio
Non-Hodgkin lymphoma	15	3005 ± 499	214 ± 63	14.0
Breast Ca	13	4105 ± 1092	519 ± 156	7.9
Renal Ca	12	3777 ± 582	348 ± 49	10.9
Pheochromocytoma	5	7852 ± 876	446 ± 280	17.6
Medullary thyroid Ca	5	2173 ± 555	100 ± 100	21.8
Ileal NET	4	8470 ± 944	2285 ± 905	3.8
Small cell lung Ca	4	7759 ± 1294	1722 ± 718	4.5
Paraganglioma	2	10,000 ± 0	641 ± 169	15.6

$SSTR_2$ peptide antagonists known (there are non-peptide antagonists as well; see the excellent review of Günther et al. on this subject [16]). Although the SSTR antagonists appear to be in principle superior than the known agonists for imaging and therapy (with **α**- or **β**-emitters), their poor internalization rates preclude the use of Auger electron-emitting labels with these ligands in radiotherapeutic applications [21, 29, 30].

4.2.3 Somatostatin Receptors: Signal Transduction

The SSTRs modulate cellular function through multiple pathways, coupled to G-protein-dependent signaling avenues. The different signaling pathways activated by the various SSTR subtypes vary according to the receptor subtype and tissue localization. The enzyme adenyl cyclase is inhibited in all SSTR subtypes, thus leading to a decrease in c-AMP production, upon ligand binding. A second signaling pathway that is activated following engagement of almost all SSTR subtypes (exception: $SSTR_1$) is the activation of G-protein-regulated inward rectifier K^+ channel. The K^+ channel activation depolarizes the cell membranes, followed by a decrease in the intracellular Ca^{2+} concentration through a decrease of Ca^{2+} efflux via the voltage-dependent Ca^{2+} channels. The reduction of the intracellular c-AMP and Ca^{2+} concentrations explains the inhibitory effects of SST in neurotransmitter and hormone secretion. A third pathway linked to SST signaling is the regulation of protein phosphatases. Upon binding to its receptor, SST activates a number of protein phosphatases from different families including serine/threonine phosphatases, tyrosine phosphatase (i.e. SHP-1 and SHP-2), Ca^{2+}-dependent phosphatases (i.e. calcineurin), and protein kinases (i.e. MAP kinase). An overview of the SST bioactivity through the various receptor subtypes can be seen in Table 4.4.

SST inhibits various secretory processes in most cases and these antisecretory effects on hormones (i.e. growth hormone, adrenocorticotropin, glucagon, and insulin), IFN-**γ**, and gastric acid are to a large extent mediated by the $SSTR_{2a/2b}$ subtype, although the $SSTR_5$ subtype inhibits the secretion of amylase. An exception to the SST antisecretory activity is the stimulation of IgM secretion ($SSTR_{2a/2b}$ subtype mediated). These effects occur within seconds to minutes after the SST-SSTR interaction. Finally (Fig. 4.5), the SSTRs mediate either the cellular antiproliferative activity through blocking degradation of the cyclin-dependent kinase inhibitor p27kip1, leading to cellular growth arrest or proapoptotic behavior (i.e. through the BAX/caspases induction).

A common theme that accompanies the GPCR-ligand interaction is its internalization, depending on the ligand concentration, the exposure time, and the parallel operation of other signaling systems. The $SSTR_{2-5}$ subtypes are internalized more efficiently than $SSTR_1$, and since $SSTR_{2a/2b}$ are the major subtypes in various tumors, this fact is of utmost importance in the design of appropriate radiotherapy (with Auger/internal conversion electron-emitting radionuclides) or chemotherapy (SST analogues linked to cytotoxic agents) approaches. The observed SSTR downregulation that accompanies the administration of SST/SST-analogues (agonists) is of critical importance in determining the amount of tumoral uptake of radiolabeled SST-analogues, and besides imaging, it has an adverse effect on tumor therapy (including radiotherapy). The time frame for the desensitization and therapy resistance occurrence (tachyphylaxis) usually ranges from hours to weeks, although the development of tumor resistance to therapy with various somatostatin analogues can take years. In experimental models of tumors treated with either continuous infusion or with b.i.d. dosing of the somatostatin analogue, the SSTR expression was dependent on the administration conditions, leading to either upregulation or downregulation respectively. A summary of the mechanisms that lead to tachyphylaxis and resistance to somatostatin analogues therapy of SSTR-expressing tumors is shown in Table 4.5.

Table 4.4 Summary of the receptor family subtypes, their localization, and their biological effects mediation [2, 9, 11]

Receptor	$SSTR_1$	$SSTR_{2a/2b}$	$SSTR_3$	$SSTR_4$	$SSTR_5$
# of amino acids (MW: kDa)	**391 (42.7)**	**369/356 (41.3)**	**418 (45.9)**	**388 (41.9)**	**364 (39.2)**
Gene location	**14q13**	**17q24**	**22q13.1**	**20p13.3**	**16p13.3**
Signalling pathways					
G-protein coupling	+	+	+	+	+
Adenyl cyclase activity	↓	↓	↓	↓	↓
Phosphotyrosine phosphatase activity	↑	↑	↑	↑↓	↑
MAP kinase activity	↑	↑↓	↑↓	↑	↓
K^+ channels	–	↑	↑	↑	↑
Ca^{2+} channels	↓	↓	–	–	–
Na^+/H^+ exchanger	↓	–	↓	↓	–
AMPA/kainate glutamate channels	↑	↓	–	–	–
PLC/IP_3 activity	↑	↑	↑	↑	↑↓
PLA_2 activity	–	–	–	↑	–
Secretion					
GH	↓	↓	–	↓	↓
Insulin	–	↓	–	–	–
Glucagon	–	↓	–	–	–
ACTH	–	↓	–	–	–
Ghrelin	–	↓	–	–	–
IFN-γ	–	↓	–	–	–
IgM	–	↑	–	–	–
Amylase	–	–	–	–	↓
Gastric acid	–	↓	–	–	–
Cellular effects					
Proliferation	↓	↑↓	↓	↑↓	↓
Apoptosis	–	↑	↑	–	–
Tissue distribution SSTRS 1–4 are almost ubiquitous in their cellular expression	Brain, pituitary, pancreas, stomach, liver, kidneys	Brain, pituitary, pancreas, stomach, lymphocytes, liver, kidneys VSMC	Brain, pituitary, pancreas, T-cells, stomach	Brain, pituitary, pancreas, stomach, placenta, lungs	Lymphoid cells, pituitary, pancreas, stomach

4.3 An Overview of Atomic/Nuclear De-excitation: Internal Conversion and Auger Electrons

The established model describing the atomic structure dictates the presence of an electron cloud surrounding a positively charged nucleus. These constituents of atoms occupy discrete energy levels and can exist in either an excited or a ground state. The excited states originate from either exogenous processes (i.e. particle or radiation bombardment) or this can be an inherent property of certain isotopes (radioactive decay) [3, 31–33].

In the majority of cases, the excited state of a daughter nucleus, formed by **α**- or **β**-decay of a parent radionuclide, rapidly proceeds via electromagnetic processes to states of lower energy (eventually to the ground state) in the daughter.

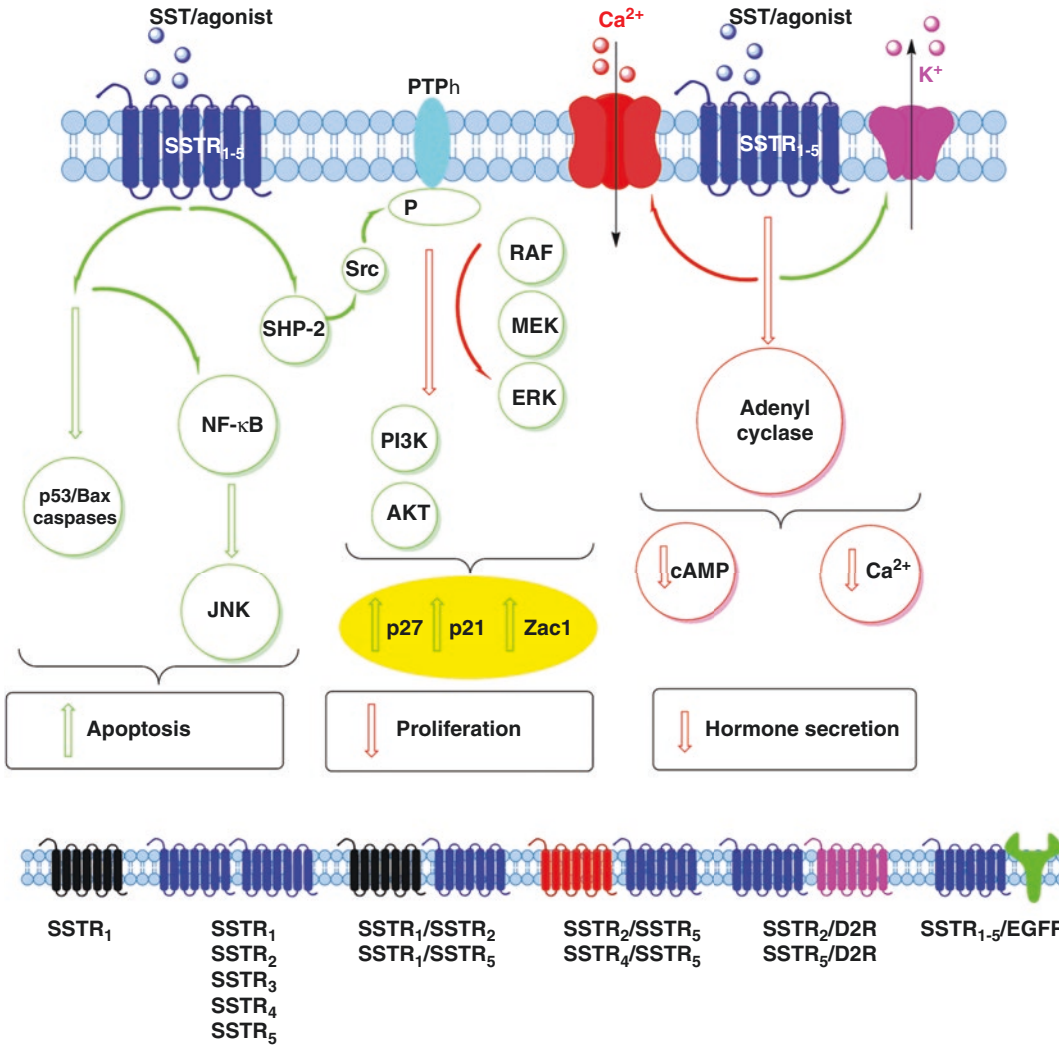

Fig. 4.5 The SST-SSTR-mediated modulation of signaling cascades leading to changes in hormone secretion, apoptosis and cell growth. In most cells, SST inhibits hormone as well as other secretions. SST cell growth and apoptosis are G protein-mediated. Phosphotyrosine phosphatases, such as SHP-1, are activated, leading to dephosphorylation of signal-transducing proteins. SST-induced inhibition of ERK blocks the degradation of the cyclin-dependent kinase inhibitor p27, leading to growth arrest. In rare cases, SST can stimulate proliferation (modified from Barbieri et al. [2, 9, 11]). AC: adenyl cyclase; PI3K: inositol trisphosphate kinase

Table 4.5 Proposed mechanisms of tachyphylaxis and resistance to SST-analogue therapy in patients with SSTR-positive tumors [2, 31]

1. Downregulation: Decrease in the number and/or affinity of SSTRs
2. Desensitization: Decrease in responsiveness due to receptor uncoupling from secondary messenger activation
3. Nonhomogeneous expression of SSTRs in tumors: outgrowth of SSTR (−) cell clones
4. Resistance due to the absence of SSTRs subtypes with high affinity for octapeptide SST analogues
5. Resistance due to tachyphylaxis of the inhibitory effect of SST analogues on direct tumor growth-promoting mechanisms (i.e., GH or gastrin secretion)
6. Mutations on SSTRs genes leading to the absence of functional receptor proteins

This de-excitation process results in the emission of either **γ**-rays or conversion electrons. Long-lived isomeric states may also decay to lower energy states in the same nucleus via electromagnetic transitions. The energy of the **γ**-ray emitted by a nucleus in a transition from a higher to a lower energy level equals to the energy difference between the two levels minus the nuclear recoil energy, which is considered negligible, except for the case of high-energy transitions of light nuclei. The emitted conversion electrons are orbital electrons of the *same* atom (internal conversion), and this de-excitation mechanism competes with the electromagnetic de-excitation process (**γ**-ray emission). In the internal conversion, the energy difference between the initial and final states in the nucleus is transferred *directly* (without a real intermediate **γ**-ray emission) to a bound orbital electron of the *same* atom, which is then ejected from its orbit, leaving an electronic vacancy behind. The ejected conversion electrons have discrete energies (linear spectrum) and this is another important difference from the electrons of the beta decay, which originate in the nucleus of the atom and have a continuous energy spectrum up to a maximum (E_{max}).

The internal conversion process should not be confused with the superficially similar photoelectric effect, which also results in an inner shell electronic vacancy. In this context, when a **γ**-ray emitted by an excited nucleus (in this case the emitted **γ**-ray photon is real!) hits a *neighboring* atom, occasionally it gets absorbed (photoelectric effect), thus producing a photoelectron of well-defined energy (this process is also known as "*external conversion*"). During the radiative transitions, the created electronic vacancy moves stepwise to a higher major shell, with no change in the number of vacancies. However, during the nonradiative transitions the number of vacancies increases by one in each step. Hence, as the innermost vacancy percolates toward the valence shell, a cascade phenomenon develops with corresponding vacancy multiplication and emission of numerous low energy electrons, collectively referred to as Auger electrons [33].

For a particular transition, the ratio of the probability for emission of an X-shell electron (X: K, L, M, etc.) to the probability for emission of the competitive **γ**-ray is called the X-shell internal conversion coefficient **α** (**α = # of de-excitations via electron emission/# of de-excitations via γ-ray emission**). The internal conversion coefficients for the different atomic shells and subshells depend on the transition energy, the atomic number of the nucleus, and the so-called transition multipolarity, which is determined by the spin-parity change between the initial and final states in the nucleus (Weisskopf rules). In general, the internal conversion coefficient for a particular atomic shell or subshell increases with decreasing transition energy (as long as the particular internal conversion process is energetically allowed), increasing atomic number, and increasing transition multipolarity. Internal conversion is often negligible for transitions in light nuclei but may occur with nearly 100% probability in isomeric transitions with high multipolarity or in low-energy transitions in heavy nuclei [3, 33].

Usually, the internal conversion coefficient for a given transition is largest for the innermost shell, for which internal conversion is energetically possible and decreases for each higher shell. Exceptions occur, however, for transition energies slightly greater than the binding energy of an atomic shell. If the spins of the initial and final states are both zero, the quantum mechanical rules (conservation of angular momentum) prohibit this electromagnetic transition ($\Delta I = 0$) and therefore the de-excitation via a *single* **γ**-ray emission is strictly forbidden (emission of two **γ**-rays is a possibility though, but this de-excitation mechanism is insignificant). In this case, if the energy difference of the two states (ΔE) is <1.022 MeV, the internal conversion is the only de-excitation mechanism. However, if ΔE is ≥1.022 Mev, then the de-excitation via a positron-electron pair production is also feasible [3, 33].

The nuclear decay processes of electron capture (EC) and the production of conversion electrons (CE) always produce a vacancy in an inner

atomic orbital, thus leaving the atom (*not the nucleus*) in an excited state and positively charged. The relaxation to the ground state is a rapid process, via either radiative (through emission of characteristic X-rays) or nonradiative processes, known collectively as Auger processes. Auger processes result in the emission of Auger, Coster-Kronig (CK), and super-CK electrons, as their ejection leaves the atom highly charged (positive). These are distinguished by the shells involved in the transition and the ejected electrons are often collectively referred to as Auger electrons [3, 33].

Although the Auger emission process was initially observed and published in 1922 by Lise Meitner, it was also independently discovered by the French physicist Pierre Victor Auger in 1923. In his experimental work, high-energy X-rays were used to ionize gas particles (argon) and the emitted photoelectrons were studied using a Wilson cloud chamber. It was observed that the emitted Auger electrons always originated from the same point (orbital vacancy) that the photoelectron generated from the interaction of the incident X-ray photon and the argon atom. If the Auger effect were a two-step phenomenon, requiring the prior emission of an X-ray photon *before* the Auger electron emission, the emitted X-ray (originating from the argon atom) should have to travel a finite distance, and in this case the Auger electrons would appear at some other point along its track. However, this was not observed to be the case and the concept of a radiationless process was invoked to explain the mechanism of the Auger electron generation [3, 33, 34].

The Coster-Kronig transition is a special case of the Auger process in which the ejected electron carries the energy of a transition within the *same shell* (same principal quantum number **n**), but it is ejected from a *higher subshell* (with different orbital quantum number **ℓ**). Furthermore, the super Coster-Kronig transitions occur within the *same subshell* (same principal quantum number **n** and same orbital quantum number **ℓ**) and the energy difference is imparted on the ejected electron originating from the *same subshell*. It is understood that this cascade of events continues until the only remaining vacancies are in the outermost electron shell. The above described processes are competitive processes, with radiative relaxation being more probable for K-shell vacancies and nonradiative relaxation being more probable for vacancies in the L-shell and above (see Fig. 4.5). Most of these Auger electrons have very low energies (20–500 eV) with ranges (1–10 nm) in living tissues and like the internal conversion electrons, the Auger electrons have also discrete energies, resulting in a sharp energy peak spectrum. The entire Auger electron cascade is completed within 1 fs (10^{-15} s) [33] (Fig. 4.6).

The explanation of the Auger effect and the internal conversion processes stems from the quantum-mechanical description of the atomic world. From this perspective, due to the fact that the wave functions of the nuclei and electrons are allowed to overlap (the nonlocality principle), the *direct* energy transfer (quantum-mechanical coupling) to the ejected Auger or conversion electrons is feasible without the prior emission of a photon (X-ray or **γ**-ray respectively).

The observation that the Auger electrons are highly radiotoxic, by pioneers in the field like Feinendegen [35] and Howell [36], took approximately two decades to mature for applications in tumor radiotherapy. The Auger electron radiotoxicity, summarized by their high-LET (LET: Linear Energy Transfer: 4–26 keV/μm), low-energy (≤1.6 keV), and short-range (≤150 nm electrons), is caused by multiple ionizations in the immediate vicinity (within a few nanometers) of the decay site. In contrast to **α**- and **β**-particles, the Auger electrons, despite their high LET, are much less radiotoxic to healthy cells, while circulating in blood or bone marrow, but they become highly radiotoxic when incorporated or decay near the DNA of target cells (see Table 4.6 and Fig. 4.7).

The Auger electron's range in water varies from a nanometer to several micrometers, comparable with that of subcellular structures and the highly localized energy deposition (10^6–10^9 cGy) in a very small volume near the nucleus can be as cytotoxic as the **α**-particles of a Po-210 atom emitted from a point at the cell surface [33–35, 38].

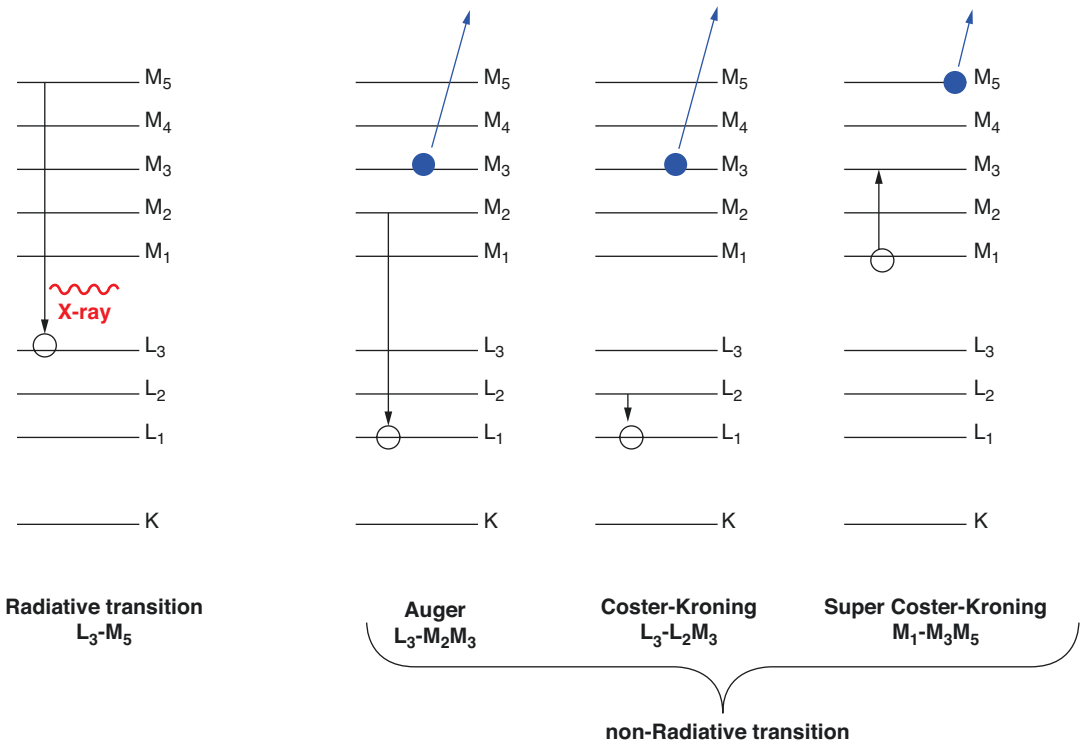

Fig. 4.6 Schematic diagram for radiative and nonradiative transitions. The ejected Auger electrons are shown in blue. In the nonradiative transitions the first two letters refer to the observed transition and the third letter refers to the subshell origin of the Auger electrons [3, 33]

Table 4.6 Radioisotope characteristics for radiotherapeutic applications [31]. *LET* Linear Energy Transfer, *EC* Electron Capture, *IC* Internal Conversion

Decay mode	Emitted particles[a]	$E_{min} - E_{max}$	Range	LET
α-decay	Helium nuclei (1)	5–9 MeV[b]	40–100 μm	≈80 keV/μm
β-decay	Energetic electrons (1)	50–2300 keV[c]	0.015–12 mm	≈0.2 keV/μm
EC/IC	Nonenergetic electrons (5–30)	ev-keV[b]	2–500 nm	≈4–26 keV/μm

[a]Number of particles
[b]Monoenergetic
[c]Average energy (continuous energy spectrum up to a maximum E_{max})

DNA is the principal target responsible for radiation-induced biologic effects of the Auger electrons. The Auger electrons-DNA interaction results in number of different DNA lesions, such as single-strand breaks (SSB), double-strand breaks (DSB), base damage, DNA-protein cross-links, and multiply damaged sites (MDS). These changes may be produced by either the direct ionization of DNA (direct effect) or by the DNA interaction with free radicals (indirect effect), comprised mostly of hydroxyl free radicals (OH•) originating from the radiolysis of the nearby abundant water molecules and whose range is several nanometers (Figs. 4.7 and 4.8). Most of these lesions are repaired with high fidelity, the exceptions being DSB and MDS. Additional damage is caused from the charge neutralization of the de-excited atom, which acquires a high positive charge as the result of the Auger emission cascade [40–42].

The ideal Auger emitter for radiotherapy applications must fulfill certain criteria which are

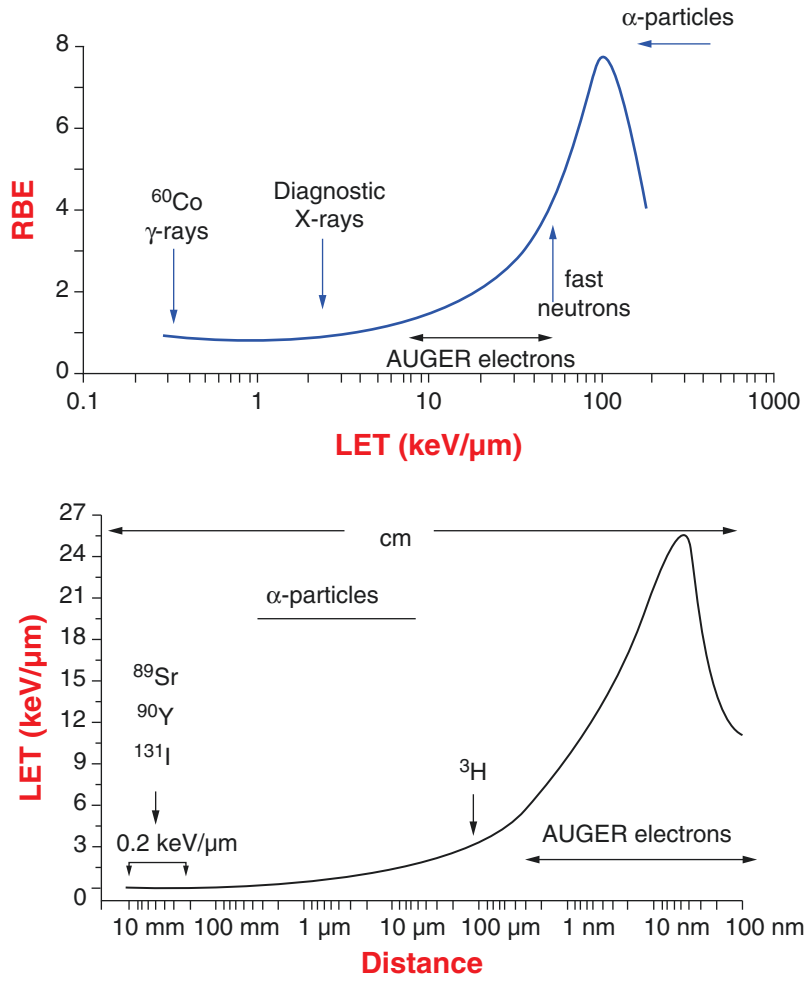

Fig. 4.7 *Upper*: Relative biological effectiveness as a function of LET (*LET* linear energy transfer) expressed in keV/μm of tissue. *Lower*: LET as a function of distance (LET refers to the *energy* absorbed by the media per unit of distance travelled by the ionizing radiation) [3, 31]

summarized in Table 4.7. The first criterion is absolutely essential to ensure the Auger emission process. The half-life range (second criterion) is based on the need for long $t_{1/2}$ in case of slow tumor uptake kinetics. Thus, a much shorter $t_{1/2,}$ combined with slow tumor uptake, will rather irradiate the surrounding normal tissues during the circulation, than the tumor. In his context, a much larger $t_{1/2}$ results in a lower radiation dose to the tumor, since the number of receptors on the tumor cells is finite and the occupancy by an appreciable number by non-emitting ligands will result in a suboptimal irradiation of the tumor cells, especially if they exhibit a rapid proliferation rate. The third criterion is needed to avoid the normal tissue irradiation and especially the rapidly dividing bone marrow cells. However, a low-intensity photon emission in the 100–200 keV range is desirable for dosimetry calculations. The last three criteria (4–6) are essential to minimize the presence of radionuclidic impurities, originating from either the same element as the desired therapeutic radionuclide (for example, the presence of In-114m during the In-111 production) or from the radioactive decay products that could expose the normal tissues to undesirable radiation burden. The (p, n) nuclear reaction offers the opportunity for the local production of radionuclides with cyclotrons during the development and clinical trial phases. For practical reasons (availability), the isotopes Ga-67, In-111, I-123, and I-125 are currently

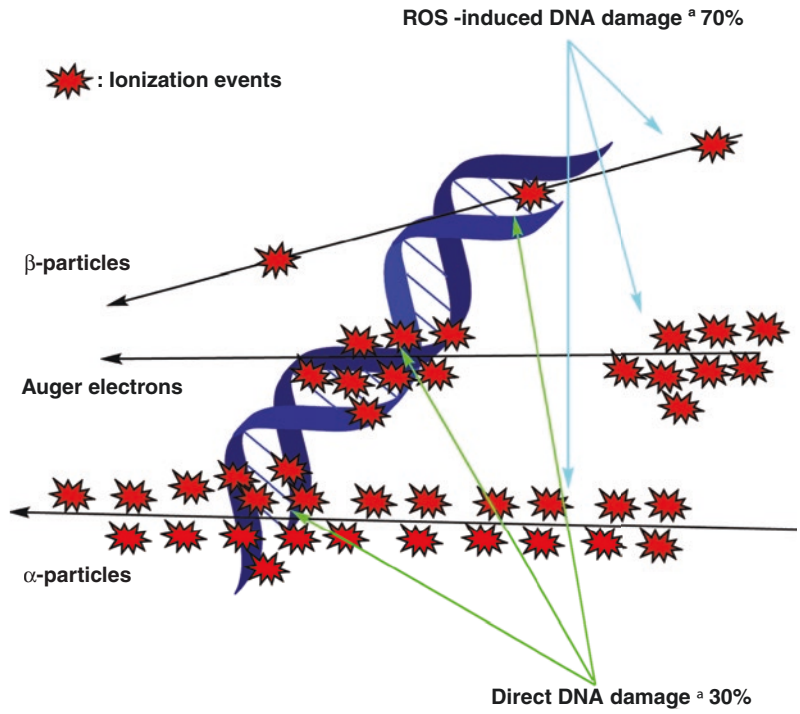

Fig. 4.8 Schematic representation of ionization density along the path of **α**-, **β**-particles, and Auger electrons (**α**-particles are considered densely-ionizing radiation, **β**-particles are sparsely ionizing and Auger electrons form clusters with a high density of ionization [37, 39–41]. *ROS* Reactive Oxygen Species

Table 4.7 A tabulation of the most important characteristics of Auger-emitting radionuclides for tumor therapy applications

Desirable properties of Auger-emitting radionuclides	
1.	Radioisotope must decay either via EC or IT (IT: internal transition) decay
2.	3 h < $t_{1/2}$ < 5 days
3.	Low abundance of emitted γ-photons
4.	Production via the (p, n) nuclear reaction
5.	Preferably no other co-existing nuclear states of the isotope
6.	Stable or very long half-life of daughter nuclide
7.	Chemical properties for easy synthesis of the appropriate labeled vectors

considered for Auger electron radiotherapy applications, despite the fact that they do not fulfill all the above criteria [32, 43, 44].

Many radionuclides decay by electron capture and/or internal conversion and therefore inevitably emit Auger electrons with energies ranging from a few eV to a few keV. In Table 4.8 the internal conversion and Auger-emitting parameters are listed for a few of commonly used radioisotopes. From this table, it is obvious that the total energy deposition per decay is the highest for In-111, thus making this isotope appropriate for tumor therapy applications, despite its limitations, mostly appropriate for the treatment of micrometastases or small-volume metastatic foci. It has been shown that in therapy of neuroendocrine tumors with [111In-DTPA0-D-Phe1]-Octreotide, it is the Auger electrons that are responsible for the observed tumoricidal effects and not the high-energy conversion electrons (145–245 keV) [25, 32].

The ongoing research effort has been exploring the potential of other CE/AE-emitting isotopes for radiotherapeutic applications, such as Pt-193m/Pt-195m, Sb-119, and Cu-64. However, radioisotope availability (for example, Pt-195m is not available in carrier-free form, although with 33 emitted electrons/decay, it has the highest Auger electron yield known), lack of convenient and/or appropriate chemistry or cost-related considerations, have hampered these efforts so far, leaving as practical choices In-111 (8 Auger electrons/decay), I-125 (21 Auger electrons/decay), and I-123 (11 Auger electrons/decay) and

Table 4.8 Auger (AE) and conversion electron (CE) emission parameters of some commonly used radionuclides

Parameter	I-125	In-111	I-123	Tc-99m	Ga-67	Tl-201
Half-life (days)	59.4	2.80	0.55	0.25	3.26	3.04
Number of AE/decay	24.9	14.7	14.9	4.0	4.7	36.9
AE energy/decay (keV)	12.2	6.8	7.4	0.9	6.3	15.3
AE energy range (keV)	0.02–30.3	0.04–25.6	0.02–30.35	0.2–17.8	0.9–9.4	0.07–66.9
Range of AE in water	1.5 nm–14.0 μm	0.25 nm–13.6 μm	0.5 nm–13.5 μm	13 nm–6.5 μm	0.1–2.7 μm	3 nm–40 μm
Number of CE/decay	0.9	0.2	0.2	1.1	0.3	1.1
CE energy/decay (keV)	7.2	25.9	20.2	15.4	28.1	30.2
CE energy range (keV)	3.7–35	145–245	127–159	100–140	82–291	1.6–153
Range of CE in water (μm)	0.7–16	205–622	100–130	70–112	50–300	0.2–126
Associated γ-emissions (keV)	35	171.3, 245.4	159.0	140.5	9.1, 9.3, 184, 209, 300, 393	135.3, 167.4
Total energy/decay (keV)	61.4	419.2	200.4	142.6	201.6	138.5
Total energy deposited/decay ($\times 10^{-14}$ Gy kg/Bq/s)	1.0	7.0	3.2	2.3	3.14	2.2

even Ga-67. It has to be emphasized though, that there are significant differences in the Auger yields reported in the literature and most of these difference can be attributed to the lack of detailed knowledge of the relevant atomic transition rates, most prominently in the outer (*M*, *N*, etc.) shells. In addition, another important consideration for the Auger emitter choice is not only the number of emitted electrons per decay but also the residence time of the Auger emitter inside the cell, so that the energy deposition from its decay would have the expected tumoricidal effect [41–46].

4.4 The In-111 Decay Pathway

Indium (In-111) is a cyclotron-produced radioisotope (Curium, France, formerly Mallinkcrodt BV, the Netherlands) by the proton irradiation of a cadmium (Cd-112)-enriched target, via the reaction: [^{112}Cd (p, 2n) ^{111}In]. This production path is preferred over the alternative reaction [^{111}Cd (p, n) ^{111}In], which is accompanied by the co-production of high levels of In-111m as an undesirable radionuclidic impurity [47, 48]. At the time of calibration, the preparation contains not less than 99.925% In-111 and not more than 0.075% In-114m and Zn-65 combined. At the time of expiration, it contains not less than 99.85% In-111 and not more than 0.15% In-114m and Zn-65 combined. At the time of calibration, the no carrier added (n.c.a.) Indium (In-111) Chloride sterile solution in dilute HCl acid (0.02–0.05 N) contains not less than 95% of the Indium present in the In^{3+} ionic form, while any metal impurities (tested: Cu, Fe, Cd, Pb, Zn, Ni, Hg) are below ppm levels. Indium (In-111) decays by electron capture (EC) to cadmium (Cd-111), a stable isotope, with a physical half-life of 67.32 h (2.8049 days). A detailed In-111 decay map is shown in Fig. 4.9.

The In-111 decay to the ground state of Cd-111 (stable) proceeds not directly, but through three intermediate steps, since the direct transition

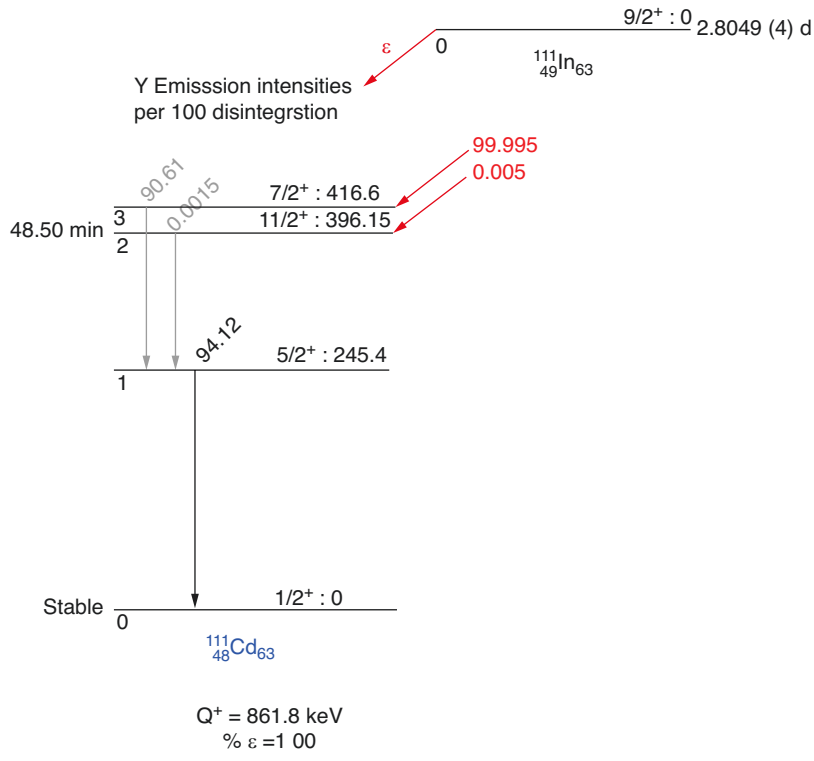

Fig. 4.9 The decay diagram of In-111 by EC. Note the nuclear spin changes of the transition levels [35, 49]

Table 4.9 Energy, yield, and range of photons and particles emitted by decaying In-111 nuclei. Very low energy photons and electrons are omitted [35, 45, 46]

Radiation	E (keV)	Yield/ decay	Range (μm)
Auger electrons			
Auger KLL	19.1	0.1030	8.21
Auger KLX	22.3	0.0394	10.8
Auger KXY	25.5	0.0036	13.6
Auger LMM	2.59	0.835	0.287
Auger LMX	3.06	0.190	0.375
Auger LXY	3.53	0.109	0.473
Auger MXY	0.35	2.09	0.0164
Auger NXY	8.47×10^{-3}	7.82	2.51×10^{-4}
Coster-Kroning electrons			
CK-LLX	0.183	0.151	8.69×10^{-3}
CK-MMX	0.125	0.915	6.35×10^{-3}
CK-NNX	0.0183	2.54	2.50×10^{-3}
Conversion electrons			
IC 1 K	145	0.0824	2.05×10^{-3}
IC 1 L	167	0.0100	2.72×10^{-3}
IC 1 M, N, …	171	0.0140	2.83×10^{-3}
IC 2 K	219	0.0521	5.20×10^{-3}
IC 2 L	241	0.0091	6.09×10^{-3}
IC 2 M, N, ….	245	0.0019	6.22×10^{-3}
X-rays			
X-ray $K_{\alpha 1}$	23.2	0.4630	–
X-ray $K_{\alpha 2}$	23.0	0.2400	–
X-ray $K_{\beta 1}$	26.1	0.0788	–
X-ray $K_{\beta 2}$	26.6	0.0186	–
X-ray $K_{\beta 3}$	26.1	0.0382	–
X-ray $K_{\beta 5}$	26.3	0.0011	–
X-ray L	3.23	0.0499	–
X-ray M	0.356	0.0030	–
γ-Rays			
γ-1	171	9.06×10^{-1}	–
γ-2	245	9.37×10^{-1}	–

from In-111 → Cd-111 ($I = 9/2^+ \rightarrow I = 1/2^+$) with a single γ-ray emission is strictly forbidden on quantum mechanical grounds ($\Delta I = 4$).

- **Step1:** The transition from the energy level of Indium-111 to the 416.6 keV excited state of Cd-111 via an electron capture process, accompanied by K X-ray emission in 71.7% of the transitions, with the other 28.3% consisting of conversion and Auger electrons and low energy photons.
- **Step 2: The** transition from the 416.6 keV excited state of Cd-111 to its 245.4 keV excited state; in the 90.6% of these transitions 171 keV **γ**-rays are emitted. In the other 9.4% of transitions, a conversion electron is produced, followed either by K X-rays (71.7% of the transitions) or by Auger electrons and low-energy photons (in 28.3% of the transitions).
- **Step 3: The** transition from the 245.4 keV excited state of Cd-111 to its ground state; 94.1% of these transitions consist of 245.4 keV **γ**-rays. In the other 5.9% of transitions, a conversion electron is produced and that is followed either by K X-rays (in 71.7% of cases) or by Auger electrons and low-energy photons (in 28.3% of the transitions).

The 171.3 and 245.4 keV **γ**-rays of Cd-111 de-excitation are used for imaging; the energy, range, and yield per decay of Auger and the conversion electrons emitted and responsible for tumor radiotherapy effects are shown in Table 4.9.

4.5 A Brief Reminder of Indium Chemistry

Indium is a group (IIIA), p-block metal like Gallium (Ga) and Thallium (Tl) and its most stable oxidation number is +3. In^{3+} is a Lewis acid and according to the Pearson HASB (HASB: Hard Acid-Soft Base) classification it is considered a hard acid ($I_A = 6.30$ for In^{3+}). In^{3+} exhibits marked similarities with Fe^{3+}, although Fe^{3+} is a harder acid ($I_A = 7.22$ for Fe^{3+}) than In^{3+} (the larger the parameter I_A, the harder the acid). The radiochemistry of indium is fairly straightforward and it deals with the metal ion in its stable In^{3+} form and in complexes with coordination numbers usually 6 or 7 (range: 4–8). There is generally little **π**-bonding to stabilize the indium–ligand bond and in the presence of monodentate ligands (i.e. acetate) there is a tendency for these complexes to undergo rapid ligand exchange reactions. The desired kinetic stability for the synthesis of radiopharmaceuticals can be

achieved only through the use of polydentate ligands, preferably those with substituents that provide steric shielding [50–56].

In acidic aqueous solutions, for example in aqueous HCl solution (0.1 M HCl), the mixed octahedral indium In^{3+} complexes $[In(H_2O)_4Cl_2]^+$ and $[In(H_2O)_5Cl]^{2+}$ prevail. These species are weak complexes with small affinity constants ($\log k_a = 3.84$ and $\log k_a = 2.58$ respectively) and highly labile, since the H_2O and halide ligands are exchanged rapidly moving from the inner coordination sphere of the indium ion to the solution and vice versa. In the case of the complexation of In^{3+} by citrate in acidic conditions, a complex mixture of species is formed. Taking into account the very low $[In^{3+}]$/[citrate] ratio during the preparation of various radiopharmaceuticals, the labile citrate complex $[InH_2Cit]^+$ with $\log k_a = 5.20$ ($\log k_a = 6.80$ has also been reported, although both values are of questionable validity) is the most likely species. It is reminded that the magnitude of the affinity constant reflects the ΔG change of the reaction (for $\Delta G < 0$, $k_a > 1$) [57, 58]. It should be kept in mind that ΔG is a thermodynamic parameter, while the lability or inertness of the formed complex is a kinetic parameter and it reflects the magnitude of the activation energy (E_a) of the rate-limiting step of the reaction mechanism. In radiochemistry, besides the thermodynamic stability, the kinetic inertness of the radiopharamaceutical is the other parameter of utmost importance. In the case of the Indium-DTPA complexes, their kinetic stability dictates their behavior in vivo (after the IV administration), where these complexes encounter transferrin, an iron-binding blood plasma glycoprotein with a high plasma concentration (0.25 g/100 mL). Transferrin has two Fe^{3+} binding sites (respective affinity constants: $\log K_{a1} = 30.5$ and $\log K_{a2} = 25.5$), and it is normally saturated only by 20–30% with iron ions, therefore, it is capable of sequestering any other radiometal present that can form complexes with, including In^{3+} [59].

Fortunately, the sequestering of In^{3+} from its Indium-protein conjugates to transferrin at physiological pH is a quite slow process. Being otherwise, these complexes would be useless for radiopharmaceutical applications. In fact, Yeh et al. [60] showed an In-111 label transfer rate from a ^{111}In-DTPA-HSA conjugate to transferrin of 1.6% per day at physiological pH and 37 °C (HSA: Human Serum Albumin), which was only slightly lower (2.6%) than the transfer rate of the In-111 label from the ^{111}In-DTPA complex to transferrin. In the case of benzyl-EDTA-HSA and phenyl-EDTA-HSA, which are sterically hindered ligands for the $^{111}In^{3+}$ complexation and more lipophilic, the transfer rate of the In-111 label from these complexes to transferrin drops to 0.11% and 0.060 respectively. The exceptional stability of ^{111}In-DTPA-fibrinogen towards transferrin transchelation of the $^{111}In^{3+}$ label was also shown from 24 h incubation experiments of this compound in serum at 37° C [61].

As mentioned before, Indium ion is a hard acid; therefore it forms complexes with a wide variety of organic ligands, especially with nitrogen, oxygen, or charge-carrying oxygen atoms (hard bases). Indium complexes of interest in the radiopharmaceutical field are based on the N_3O_5 or N_4O_4 motif of aminocarboxylate ligands (i.e. DTPA, DOTA), which exhibit very high affinity or formation constants ($\log k_a = 28.4$ for the In-DTPA complex). It should be noted though that even S-containing ligands (i. e. aminothiol: **-N-CH_2-CH_2-S^-**) have been prepared with even higher affinity constants ($\log k_a > 33$), despite the "softness" of the sulfur atom (sulfur has a larger atomic radius than oxygen and it is polarizable, hence its "softness") [62–64].

The In^{3+} ion is also known for its amphoteric character, and for this reason it hydrolyzes easily in aqueous solutions, forming insoluble hydroxides/colloids at pH > 3.4 (in dilute concentrations, $In(OH)_3$ does not actually precipitate). Since the In-hydroxy colloid formation occurs more rapidly than the complexation with aminocarboxylate ligands in acidic solutions (pH: 4.0–5.5), this problem is avoided through the rapid formation of an intermediate weak (and labile) complex with an appropriate chelator, such as citrate followed by a transchelation reaction with the aminocarboxylate ligand. The citrate use is preferred, instead of an acetate-based buffer, since Indium does not precipitate or forms

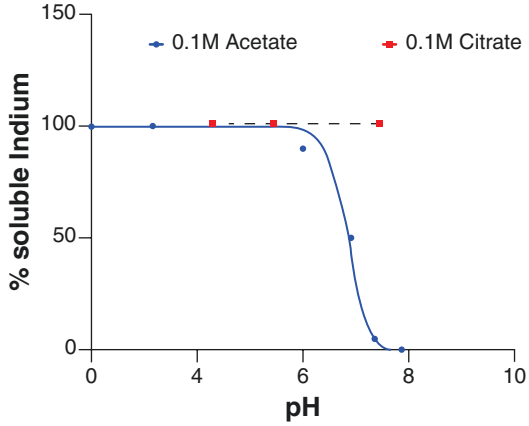

Fig. 4.10 The percentage of soluble Indium in citrate and acetate buffers, as a function of pH. Note that acetate ions are monodentate ligands, while citrate (4-dentate ligand) can form kinetically labile chelate complexes [55]

colloids at the slightly acidic solutions (pH: 4.0–5.5, see Fig. 4.10) of various radiopharmaceutical preparations [65]. Once prepared, the thermodynamically stable DTPA-Indium complexes are relatively inert, with minimal in vivo transfer of the In-111 label to transferrin [57, 61, 66, 67].

Cadmium is a ubiquitous environmental contaminant that can be encountered in syringes or vials and is also the unavoidable decay product of the In-111 label, thus competing with In^{3+} in its complexation reactions (i.e. with the DTPA moiety, $\log K_a$ = 19.1 for the Cd^{2+}-DTPA reaction). The time delay between the production of In-111 and its incorporation to the appropriate radiopharmaceutical (usually 7–11 days later), before their administration to patients, contributes to the increase of the undesirable cadmium levels in the $^{111}InCl_3$ solutions (Cd^{2+} in growth). Another problem encountered in the In^{3+} handling is its tendency to get adsorbed on glass vial walls (even a 20–30% of the dose can get adsorbed). As a result, the number of In-111 labeled DTPA-Octreotide molecules available for receptor binding is substantially decreased with adverse impact on its use as imaging or therapy agent. Therefore, it is imperative to take precautions such as use of appropriate containers and syringes during the radiopharmaceutical preparation and the use of ultrapure $^{111}InCl_3$ solution. Ideally, the purification of the $^{111}InCl_3$ solution should be done immediately prior to the complexation reaction. Such a purification method relies on column chromatography with a strong anion exchange resin (DoweX-1-chloride, 8% X-linking, 100–200 dry mesh), preconditioned with the successive passage of 10 mL of HCl (0.1 N), 10 mL of a 0.9% NaCl (for IV use) solution, and 10 mL of water for injection. Then, the crude $^{111}InCl_3$ solution is loaded on top of the resin bed and the purified $^{111}InCl_3$ eluate is collected in a sterile polypropylene vial. Since Indium-111 is commercially available in dilute hydrochloric (HCl) acid (0.2–0.5 N), the Cd^{2+} contaminant to be removed is present as an *anionic* tetrahedral complex $[CdCl_4]^{2-}$, which is retained by the column [68].

An interesting approach to maximize the $^{111}In^{3+}$ incorporation in various In-111 complexation reactions was through the use of either MES (MES: 2-(*N*-morpholino)ethanesulfonic acid) or HEPES (HEPES: 4-(2-hydroxyethyl)-1-piperazineethanesulfonic acid) as buffers. With these buffers, high specific activities of ^{111}In-labeled peptides are achieved (see Fig. 4.10), possibly due to their weak complex formation tendency with the In^{3+} ions (the HEPES and MES structures are shown in Fig. 4.11; the presence of electron-donating atoms is obvious). Moreover, when the labeling was performed in MES- and HEPES-based buffers, the labeling efficiency of ^{111}In-labeled peptides was not adversely affected by Cd^{2+} concentrations up to 0.1 nM (see Fig. 4.12). Therefore, with the use of HEPES or MES in place of citrate or acetate buffers, the time-consuming purification step of $^{111}InCl_3$ described previously can be safely avoided [69].

4.6 The Preparation of [^{111}In-DTPA^0-D-Phe^1]-Octreotide

4.6.1 The Kit Components

Octreoscan™ is a commercial kit used for the preparation of [^{111}In-DTPA^0-D-Phe^1]-Octreotide, a radiopharmaceutical (CURIUM™, France; formerly Mallinckrodt Nuclear Medicine BV, the

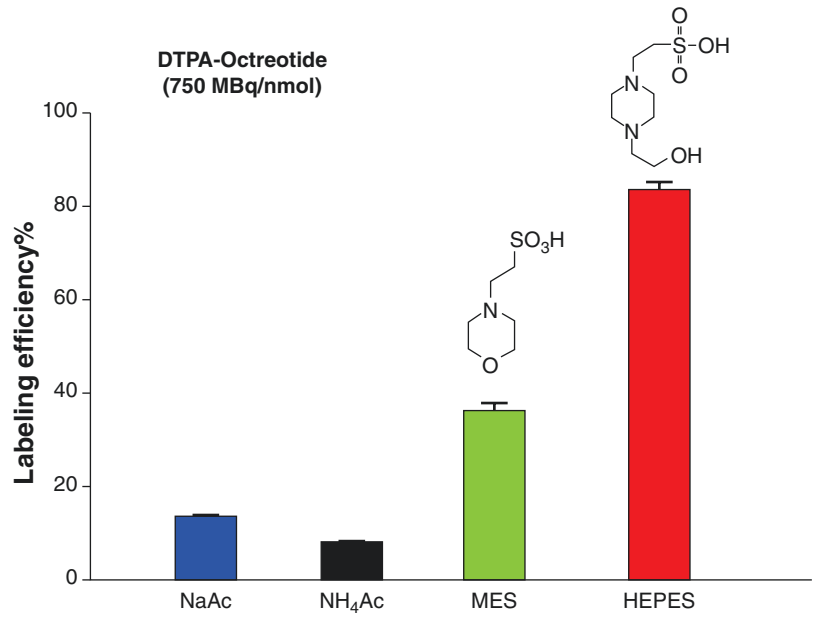

Fig. 4.11 The % ^{111}In-labeling efficiency of DTPA-Octreotide in 0.1 M NaAc, NH_4Ac, MES and HEPES buffers [69]. MES: 2-(*N*-morpholino) ethanesulfonic acid), HEPES: 4-(2-hydroxyethyl)-1-piperazineethanesulfonic acid)

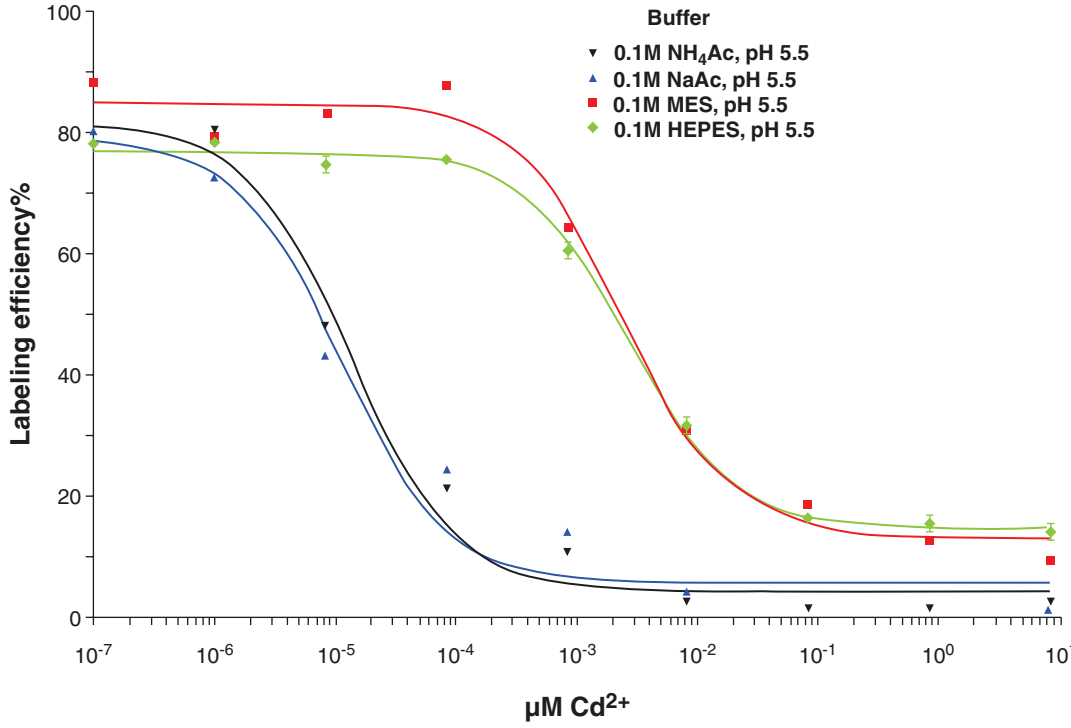

Fig. 4.12 The effect of [Cd^{2+}] on the labeling efficiency of ^{111}In-DTPA-exendin-3 in 0.1 M NaAc, NH_4Ac, MES and HEPES buffers (pH: 5.5) [69]. MES: 2-(*N*-morpholino) ethanesulfonic acid), HEPES: 4-(2-hydroxyethyl)-1-piperazine ethanesulfonic acid)

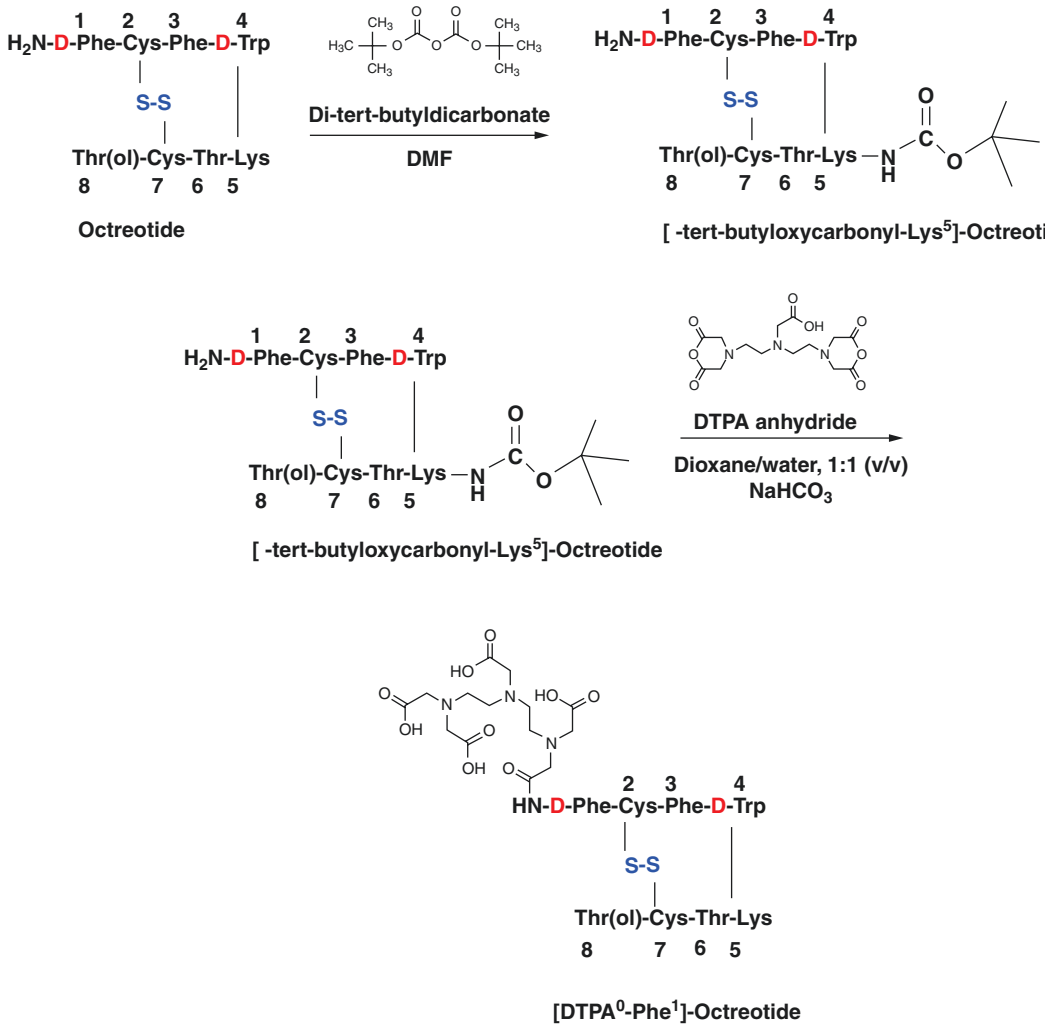

Fig. 4.13 Reaction scheme for the synthesis of [DTPA^0-D-Phe^1]-Octreotide. Replacement of Phe^3 in Octreotide by Tyr^3 (which can be easily radioiodinated) leads to an analogue with improved $SSTR_2$ affinity, but the $SSTR_3$ and $SSTR_5$ affinity is reduced; the C-terminal presence of Thr instead of Thr(ol) results in a $SSTR_2$-selective ligand with a sevenfold improvement of $SSTR_2$ affinity [73]

Netherlands) approved for diagnostic applications. The same kit can be also used for radiotherapeutic applications, although in this case, much higher total doses must be administered [70, 71]. This kit consists of two components:

Vial 1: The 10-mL Octreoscan™ Reaction Vial 1 contains a lyophilized mixture of:

1. 10 μg [DTPA^0-D-Phe^1]-Octreotide [*N*-(diethylenetriamine-*N*,*N*,*N*′,*N*″-tetraacetic acid-*N*″-acetyl)-D-phenylalanyl-L-hemicystyl-L-phenylalanyl-D-tryptophyl-L-lysyl-L-threonyl-L-hemicystyl-L-threoninol cyclic (2 → 7) disulfide], also known as pentetreotide,
2. 2.0 mg gentisic acid [2, 5-dihydroxybenzoic acid] as antioxidant,
3. 4.9 mg trisodium citrate, anhydrous as transfer ligand,
4. 0.37 mg citric acid, anhydrous, for buffering and
5. 10.0 mg inositol as bulking agent.

Prior to lyophilization, sodium hydroxide or hydrochloric acid is added for pH adjustment. The vial contents are sterile and nonpyrogenic, without bacteriostatic preservatives present (the information presented about the Octreoscan™ kit was obtained from the CURIUM™/Mallincrodt package insert [72]).

Vial 2: The 10-mL vial 2 of Indium In-111 Chloride sterile solution contains:

1. 1.1 mL or 111 MBq/mL (3.0 mCi/mL) of indium In-111 chloride ($^{111}InCl_3$) in 0.02 N HCl, at the time of calibration.
2. Ferric chloride ($FeCl_3$) at a concentration of 3.5 μg/mL ([Fe^{3+}] = 1.2 μg/mL), as a labeling efficiency augmenter. The vial contents are sterile and nonpyrogenic, without bacteriostatic preservatives present.

For radiotherapeutic applications, 4–5 vials of the diagnostic kit were used, with a total peptide amount 40–50 μg and total added radioactivity of $^{111}InCl_3$ ranging between 110–160 mCi (4070–5920 MBq).

4.6.2 Synthesis of [DTPA^{0}-D-Phe^{1}]-Octreotide

The synthesis of the "cold" ligand ([DTPA^{0}-D-Phe^{1}]-Octreotide) is a three-step reaction (see Fig. 4.13) [73]:

First step: Reaction of Octreotide (Sandostatin™) with di-ε-*tert*-butyldicarbonate $(Boc)_2O$ in dimethylformamide (DMF) for the protection of the ε-NH_2 group of lysine.

Second step: The Lys^{5} protected product ([ε-*tert*-butyloxycarbonyl-Lys^{5}]-Octreotide) reacts with *N*,*N*′-diethylenetriaminepentaacetic acid (DTPA). DTPA dianhydride is then coupled to the selectively protected octreotide. The [ε-*tert*-butyloxycarbonyl-Lys^{5}]-Octreotide is dissolved in dioxane/water (1/1, v/v) and after addition of 20 equivalents of $NaHCO_3$, 1.1 equivalents of the DTPA-dianhydride are added. After 5 min, the dioxane solvent is removed under reduced pressure and the remaining aqueous solution is lyophilized. Purification of the product is achieved by silica gel chromatography (Silica Gel 60) with chloroform/methanol/acetic acid 50% (7/3/1, v/v/v), in order to separate the desired [DTPA^{0}-D-Phe^{1}-Boc-Lys^{5}]-Octreotide from the contaminating double-substituted DTPA-derivative and the unreacted starting material ([ε-*tert*-butyloxycarbonyl-Lys^{5}]-Octreotide).

Third step: Deprotection of the ε-NH_2 group of lysine with trifluoracetic acid, with subsequent sequential purification on Silica Gel 60, Duolite™ ES-861 and a weak basic anionic exchanger AG4-X4 (BioRad). The eluted desired product [DTPA^{0}-D-Phe^{1}]-Octreotide is then lyophilized. The purity of the preparation can be checked either by reverse phase HPLC [mobile phase: solvent A = $H_2O/CH_3CN/H_3PO_4$ (85%)/TMAH (tetramethylammonium hydroxide, 10% in water), 90/10/0.2/4 (v/v/v/v), (pH = 2.9) and solvent B = $H_2O/CH_3CN/H_3PO_4$ (85%)/TMAH (tetramethylammonium hydroxide, 10% in water), 30/70/0.4/4 (v/v/v/v), (pH 4.0); gradient 5–95% B in 20 min; column temperature: 45 °C; flow rate: 1.5 mL/min; detection wavelength: 205 nm) or by HPTLC on Silica Gel 60 HPTLC plates.

4.6.3 Labeling of [DTPA^{0}-D-Phe^{1}]-Octreotide with $^{111}In^{3+}$

The [^{111}In-DTPA^{0}-D-Phe^{1}]-Octreotide (see Fig. 4.14) was prepared by combining the two kit components. An aliquot of the supplied Indium In-111 chloride solution was added to the vial containing the "cold" ligand [DTPA^{0}-D-Phe^{1}]-Octreotide molecule to form the [^{111}In-DTPA^{0}-D-Phe^{1}]-Octreotide labeled complex (the added radioactivity was the total radioactivity divided by the number of vials used (4 or 5). The pH of the resultant [^{111}In-DTPA^{0}-D-Phe^{1}]-Octreotide solution was between 3.8 and 4.3. No bacteriostatic preservative was present. The labeling yield of [^{111}In-DTPA^{0}-D-Phe^{1}]-Octreotide of the pooled preparations was determined prior to the administration to the patient. A method recommended for determining the labeling yield of the preparation will be described in the Sect. 4.6.4 [70, 72, 73].

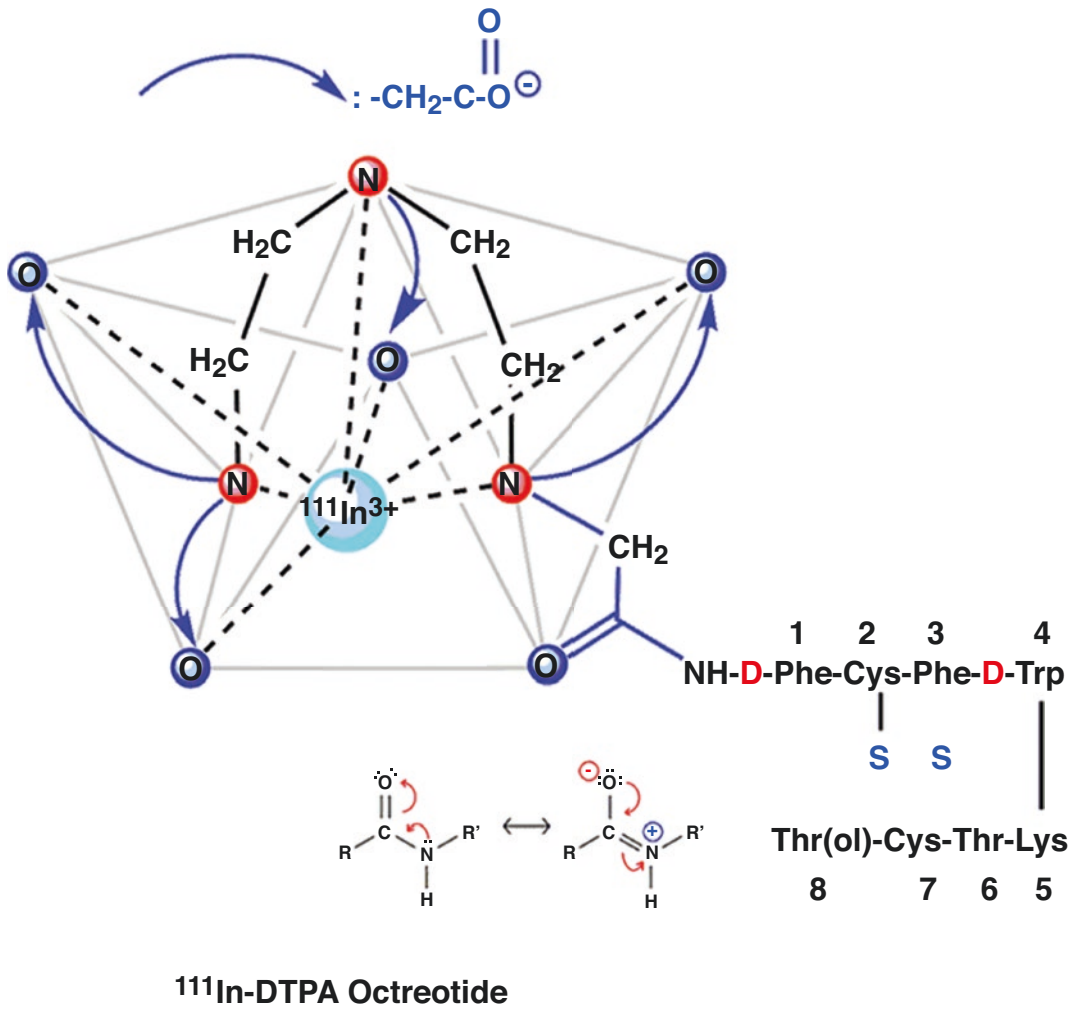

Fig. 4.14 The established distorted square antiprism geometry of the $^{111}In^{3+}$ ion with the DTPA moiety (coordination number: 7) in the [^{111}In-DTPA^{0}-D-Phe^{1}]-Octreotide molecule. The Indium atom in the above structure has been drawn off-centered to facilitate the visualization. The eighth coordination position of the $^{111}In^{3+}$ ion may interact, although weakly, with the carbonyl oxygen of the amide bond (the resonance structures of the amide bond are shown below the DTPA moiety) [74, 75]

1. An appropriate aliquot of the Indium In-111 Chloride Sterile Solution vial was aseptically removed using the needle provided only (to avoid unwanted ions that tend to leach from the needles, as Al^{3+}, Cd^{2+}, etc., in the strongly acidic solution) and a shielded, sterile syringe.
2. The Indium In-111 Chloride Sterile Solution was injected into the Octreoscan™ Reaction Vial.
3. The Octreoscan™ Reaction Vial was swirled gently until the lyophilized pellet was completely dissolved.
4. The [^{111}In-DTPA^{0}-D-Phe^{1}]-Octreotide solution was incubated at or below 25 °C for a minimum of 30 min. Note: A 30 min incubation time is required. Shorter incubation periods were avoided, as they could result in inadequate labeling.

5. Using proper shielding, the vial contents were visually inspected. The solution should be clear, colorless, and free of particulate matter. If not, the solution should not be used. It should be disposed in a safe and approved manner.
6. The [^{111}In-DTPA^{0}-D-Phe^{1}]-Octreotide pooled solution was assayed using a suitably calibrated ionization chamber.
7. The labeling yield of the pooled reconstituted vials was checked before administration to the patient, according to the instructions given below. If the radiochemical purity was less than 90%, the product was not used.
8. The reaction vial containing the pooled [^{111}In-DTPA^{0}-D-Phe^{1}]-Octreotide solution was stored at or below 25 °C (77 °F) until use and it was used within 2 h after the complexation reaction.
9. The pooled preparation can be diluted to a maximum volume of 10 mL with 0.9% Sodium Chloride Injection, USP immediately prior to injection, if desired. The sample should be drawn up into a shielded, sterile syringe and then administered to the patient.

4.6.4 Determination of the [^{111}In-DTPA^{0}-D-Phe^{1}]-Octreotide Labeling Yield [72]

4.6.4.1 Required Materials

1. Waters Sep-Pak™ C18 Cartridge, Part No. 51910
2. Methanol, 15 mL (Caution: toxic and flammable)
3. Distilled water, 20 mL
4. Disposable syringes:
   2–10-mL, no needle required
   2–5-mL, no needle required
   1–1-mL, with needle
5. Three disposable culture tubes or vials, minimum 10-mL capacity
6. Ion chamber

4.6.4.2 Preparation of the Sep-Pak™ Cartridge

1. The Sep-Pak™ cartridge was rinsed with 10 mL methanol as follows: a 10-mL syringe is filled with 10 mL methanol, the syringe was attached to the longer end of the Sep-Pak™ cartridge and the methanol was pushed through the cartridge. The eluate was discarded in a safe and approved manner.
2. Similarly, The Sep-Pak™ cartridge was also rinsed with 10 mL water. Caution was exercised, as the cartridge must kept wet, with no air bubbles trapped. If an air bubble was present, the cartridge was rinsed with additional 5 mL of water and the eluate was discarded.

4.6.4.3 Sample Analysis

1. An aliquot (0.05–0.1 mL) of the [^{111}In-DTPA^{0}-D-Phe^{1}]-Octreotide solution was withdrawn from the reaction vial, by using a 1-mL syringe. The preparation was applied to the Sep-Pak™ cartridge through the longer end of the cartridge.
2. Using a disposable 5-mL syringe, slowly (in dropwise manner) 5 mL water was pushed through the longer end of the cartridge and the eluate was collected in a counting vial. This eluate was labeled as Fraction 1.
3. Similarly, the cartridge was eluted with 5 mL methanol slowly, so that the elution occurred in a dropwise manner. This fraction was also collected in another counting vial and was labeled as Fraction 2. Two 5-mL portions of air were pushed through the longer end of the cartridge and the eluate was collected with Fraction 2.
4. The Sep-Pak™ cartridge was placed in a third vial for the assay.

4.6.4.4 Assay

1. The activity of Fraction 1 was assayed in a suitably calibrated ionization chamber. This fraction contains the hydrophilic impurities (e.g., unbound indium In-111).
2. The activity of Fraction 2 was also assayed. This fraction contained the [^{111}In-DTPA^{0}-D-Phe^{1}]-Octreotide.
3. Finally, the activity of the Sep-Pak™ cartridge was also assayed. This component contains the remaining non-elutable impurities.
4. All the materials used in the preparation, the sample analysis, and the assay were

subsequently disposed of in a safe and approved manner.

4.6.4.5 Calculations

1. Percent of [^{111}In-DTPA^{0}-D-Phe^{1}]-Octreotide = (Fraction 2 Activity/Total Activity) × 100%

   Where Total Activity = Fraction 1 + Fraction 2 + activity remaining in Sep-Pak™

   If this value was less than 90%, the preparation was not used and it was discarded in a safe and approved manner.
2. Percent of hydrophilic impurities = (Fraction 1 Activity/Total Activity) × 100%
3. Percent of non-elutable impurities = (Activity remaining in Sep-Pak™ cartridge/Total Activity) × 100%

4.6.5 Precautions

4.6.5.1 General

1. Therapy with octreotide acetate can elicit severe hypoglycemia in patients with insulinomas. Since [^{111}In-DTPA^{0}-D-Phe^{1}]-Octreotide is an octreotide analog, an intravenous line is recommended in any patient suspected of having an insulinoma. An intravenous solution containing glucose should be administered just before and during administration of [^{111}In-DTPA^{0}-D-Phe^{1}]-Octreotide.
2. Since [^{111}In-DTPA^{0}-D-Phe^{1}]-Octreotide is eliminated primarily by renal excretion, use in patients with impaired renal function should be carefully considered.
3. To help reduce the radiation dose to the thyroid, kidneys, bladder, and other target organs, patients should be well hydrated before the administration of [^{111}In-DTPA^{0}-D-Phe^{1}]-Octreotide. An increased fluid intake and frequent voiding were encouraged for 1 day after administration of this drug. In addition, a mild laxative (e.g., bisacodyl or lactulose) was recommended to the patients before and after the administration of [^{111}In-DTPA^{0}-D-Phe^{1}]-Octreotide.
4. The prepared [^{111}In-DTPA^{0}-D-Phe^{1}]-Octreotide solution should always be tested for labeling yield prior to administration. The product had to be used within 6 h of preparation.
5. Components of the kit are sterile and nonpyrogenic. To maintain sterility, it is essential that directions are followed carefully. Aseptic technique must be used during the preparation and administration of [^{111}In-DTPA^{0}-D-Phe^{1}]-Octreotide.
6. Octreotide acetate and the natural somatostatin hormone have been associated with cholelithiasis, presumably by altering fat absorption and possibly by decreasing motility of the gallbladder. However, a single dose of [^{111}In-DTPA^{0}-D-Phe^{1}]-Octreotide is not expected to cause cholelithiasis [72].

4.6.6 Adverse Reactions

The [DTPA^{0}-D-Phe^{1}]-Octreotide is derived from Octreotide, which is used as a therapeutic agent to control symptoms from certain tumors. The following adverse effects have been observed in clinical trials at a frequency of less than 1% of 538 patients: dizziness, fever, flush, headache, hypotension, changes in liver enzymes, joint pain, nausea, sweating, and weakness. These adverse effects were transient. During clinical trials, there was one reported case of bradycardia and one case of decreased hematocrit and hemoglobin. The usual diagnostic dose of [^{111}In-DTPA^{0}-D-Phe^{1}]-Octreotide is approximately 5–20 times less than the Octreotide therapeutic dose, therefore it is considered subtherapeutic, but this not the case when the [^{111}In-DTPA^{0}-D-Phe^{1}]-Octreotide is used for tumor therapy. The following adverse reactions have been associated with diagnostic doses of octreotide (10 μg of the peptide) in 3–10% of patients: nausea, injection site pain, diarrhea, abdominal pain/discomfort, loose stools, and vomiting. Hypertension and hyper- and hypoglycemia have also been reported with the use of Octreotide. The above adverse effects were more likely to occur with the administration of the 40–50 μg peptide doses used in each tumor radiotherapy session [72].

4.6.7 Dosage and Administration

For radiotherapeutic applications, 4–5 vials of the diagnostic kit were used, with a total peptide amount of 40–50 μg with the total added radioactivity of $^{111}InCl_3$ ranging between 110–160 mCi (4070–5920 MBq), depending on the patient's weight and dosimetric data. Before administration, the patient as adequately hydrated. After administration, the patient was encouraged to drink fluids liberally. Elimination of extra fluid intake will help reduce the radiation dose by flushing out unbound [^{111}In-DTPA^{0}-D-Phe^{1}]-Octreotide by glomerular filtration. It was also recommended that a mild laxative (e.g., bisacodyl or lactulose) be given to the patient starting the evening before the radioactive drug administration and it was continued for 48 h after the procedure. Ample fluid uptake was imperative during this period as a support both to renal elimination and the bowel-cleansing process.

The calculated intravenous dose of the [^{111}In-DTPA^{0}-D-Phe^{1}]-Octreotide preparation was confirmed by a suitably calibrated radioactivity ionization chamber immediately before administration. The [^{111}In-DTPA^{0}-D-Phe^{1}]-Octreotide preparation, as with all intravenously administered products, was inspected visually for particulate matter and discoloration prior to administration. Preparations containing particulate matter or discoloration were not administered and they were disposed of in a safe manner, in compliance with the regulations. Aseptic techniques and effective shielding were employed in withdrawing doses for administration to patients. Waterproof gloves were worn during the administration procedure. The [^{111}In-DTPA^{0}-D-Phe^{1}]-Octreotide was never administered mixed with TPN (TPN: Total Parenteral Nutrition) solutions or through the same intravenous line [71, 72].

4.7 Clinical Pharmacology of [^{111}In-DTPA^{0}-D-Phe^{1}]-Octreotide

[DTPA^{0}-D-Phe^{1}]-Octreotide is a DTPA conjugate of Octreotide, which is a long-acting analog of the human hormone, SST. Therefore, its labeled derivative ([^{111}In-DTPA^{0}-D-Phe^{1}]-Octreotide) binds to SSTRs on cell surfaces throughout the body. Within an hour after the injection, most of the dose of [^{111}In-DTPA^{0}-D-Phe^{1}]-Octreotide distributes from plasma to extravascular body tissues and concentrates in tumors containing a high density of SSTRs. After background clearance, visualization of somatostatin receptor-rich tissue is achieved. In addition to somatostatin receptor-rich tumors, the normal pituitary gland, thyroid gland, liver, spleen, and urinary bladder are also visualized in most patients, as is the bowel, to a lesser extent. Excretion is almost exclusively via the kidneys.

The binding of the labeled ligand [^{111}In-DTPA^{0}-D-Phe^{1}]-Octreotide to its appropriate receptor (SSTR) is followed by the internalization of the formed ligand-receptor complex via a clathrin-coated invagination of the plasma membrane, a temperature-dependent process known as receptor-mediated endocytosis. This process constitutes the major internalization pathway. The resulting vesicles shed their clathrin coat and fuse with endosomes, whose acidic environment causes the dissociation of the [^{111}In-DTPA^{0}-D-Phe^{1}]-Octreotide-SSTR complex (see Fig. 4.14). The SSTR is then recycled on the cell surface and the labeled peptide is further metabolized to ^{111}In-DTPA-D-Phe. The polarity and charge of this metabolite are responsible for its trapping inside the cell, since the ^{111}In-DTPA-D-Phe is a negatively charged molecule and therefore it cannot passively pass through the hydrophobic lysosomal or cell membranes. Moreover, part of the In-111 label may dissociate from the DTPA moiety and it migrates towards the nucleus through the nuclear pores, where it gets attached via an unknown biochemical mechanism. The emitted Auger electrons of In-111 are thus capable of releasing their energy at close proximity to the cell nucleus with high radiobiological effects (RBEs). In case the I-125-labeled Octreotide ([^{125}I-Tyr^{3}]-Octreotide) analogue is used, such a trapping is not possible, since the various I-125-containing degradation products leave the cell quite fast. In this case, the I-125 decaying atoms do not have the chance to deposit their energy in the intracellular environment, despite the high Auger electron yield per decay of I-125 and the

long half-life of this isotope, thus rendering the I-125-labeled Octreotide analogues unfit as PRRT agents (PRRT: Peptide receptor radiotherapy) [18, 25, 28, 76–80].

Besides the direct and indirect radiotoxic effects of the Auger-emitting In-111 label, after their transport inside the cells, the "bystander effect" further augments the PRRT efficacy. The "bystander effect" is mediated through the local release of cytokines and free radicals from the radiation-damaged cells, which thus induce the death in non-irradiated adjacent cells through this mechanism. The observed discrepancy between the estimated from microdosimetry and the actual radiotherapeutic effects has been partially attributed to the "bystander effect" [10, 81].

During the development phase of in vitro saturable peptide binding assays, such as receptor binding assays and radioimmunoassays, it became evident that the much needed maximization of the assay sensitivity required the highest signal-to-background noise (S/N) ratio possible. Therefore, by lowering the mass of the radioligand and/or maximizing its specific radioactivity led to the improvement in the S/N ratio [82, 83]. Octreotide belongs to the family of the regulatory peptides and consequently its respective receptors (SSTRs) are characterized by high affinity but of low capacity (therefore, they are easily saturable). In the administered labeled Octreoscan™ preparations, approximately 90% of the administered peptide is in its unlabeled form ([DTPA^0-D-Phe^1]-Octreotide), unavoidably decreasing the in vivo binding of its labeled form ([^{111}In-DTPA^0-D-Phe^1]-Octreotide), due to the anticipated competition between the labeled and the unlabeled ligands for the limited number of the same somatostatin receptor sites [84].

However, the anticipated maximum % uptake of the labeled ligand though, when the lowest possible dose of the highest specific radioactivity [^{111}In-DTPA^0-D-Phe^1]-Octreotide was administered, failed to materialize. What was in reality observed, when the % of the radioactivity uptake was plotted vs. the injected peptide mass, was a bell-shaped curve, suggesting that two opposite effects are operating in vivo. According to Breeman et al. [85], the negative effect, due to the saturation of the receptor sites when increasing total peptide amounts are present (as mentioned previously, ≈90% of the administered ligand remains unlabeled), appears to be counterbalanced by the positive effect that the higher amount of the ligand has on the endocytosis rate of the ligand-receptor complex. Thus, in order to achieve the optimum sensitivity in the scintigraphic detection of somatostatin receptor-positive tissues (i.e. tumors) an optimum dose of total peptide ligand is essential (at least 10 μg) and this has been taken into consideration in the Octreoscan™ kit formulation. It should be kept in mind though, since all the regulatory peptide receptors get saturated very rapidly, that the range of the optimal % uptake versus the injected mass of the ligand is fairly narrow; for this reason, the highest possible specific activity of the labeled ligand is absolutely essential, especially for *Peptide Receptor Radionuclide Therapy* (*PRRT*) applications, along with clinical studies for optimization of the total mass of the ligand to be administered [86]. Later results by Lewis et al. though [87], in a tumor-bearing rat model with ^{64}Cu-TETA-Tyr^3-Octreotate, seem to contradict the above interpretation of the experimental data, since in this model at least, increasing amounts of the "cold" peptide (10–5000 ng of TETA-Tyr^3-Octreotate) along with a constant amount of radioactive peptide (5 μCi/0.2 MBq ^{64}Cu-TETA-Tyr^3-Octreotate) decreased the % radioactivity uptake of the various organs, as expected (competition between "cold" and radioactive peptide for a limited number of available receptors).

Comparing the specific activities of labeled DOTA- and DTPA-peptides with In-111, Y-90 and Lu-177, the highest specific activity of the ligand was obtained with [^{111}In-DTPA^0-D-Phe^1]-Octreotide (1.7 GBq•nmole^{-1}), while the specific activity of Lu-177 and Y-90 labeled DOTA-peptides did not exceed in practice the 0.5 GBq•nmole^{-1}. The lower specific activity of Lu-177 and Y-90 labeled DOTA-peptides is believed to be the result of competing ion contaminant levels and the low DOTA-complexation reaction rate. A constraint on the maximum specific activity to be kept always in mind in the preparation of various labeled peptides is the

integrity of the labeled compound due to radiolysis, of more concern if **α**- and **β**-emitters are used, a fact that gives a definite additional advantage to the Auger-emitting labels [88, 89].

4.7.1 Pharmacokinetics

The injected [^{111}In-DTPA^{0}-D-Phe^{1}]-Octreotide leaves the plasma rapidly with one-third of the injected radioactivity dose remaining in the blood pool at 10 min after administration. Plasma levels continue to decline so that by 20 h post injection, about 1% of the radioactive dose is found in the blood pool. The biological half-life of [^{111}In-DTPA^{0}-D-Phe^{1}]-Octreotide is 6 h. Half of the injected dose is recoverable in urine within 6 h after injection, 85% is recovered in the first 24 h, and over 90% is recovered in urine by 2 days. Hepatobiliary excretion represents a minor route of elimination, and less than 2% of the injected dose is recovered in feces within 3 days after the [^{111}In-DTPA^{0}-D-Phe^{1}]-Octreotide injection [72].

4.7.2 Metabolism

For several hours after the administration of [^{111}In-DTPA^{0}-D-Phe^{1}]-Octreotide, plasma radioactivity is predominantly in its parent form. Ten percent of the radioactivity excreted is non-peptide-bound [72].

4.7.3 Pharmacodynamics

[^{111}In-DTPA^{0}-D-Phe^{1}]-Octreotide binds to cell surface somatostatin receptors. In nonclinical pharmacologic studies, the hormonal effect of Octreoscan in vitro is one-tenth that of octreotide. Since diagnostic imaging doses of [^{111}In-DTPA^{0}-D-Phe^{1}]-Octreotide are lower than the therapeutic doses of "cold" octreotide, the [^{111}In-DTPA^{0}-D-Phe^{1}]-Octreotide does not exert clinically significant somatostatin-mediated effects if administered for imaging applications, but with the radiotherapeutic peptide doses, caution should be exercised and measures should be taken to avoid any complications. [^{111}In-DTPA^{0}-D-Phe^{1}]-Octreotide is cleared from the body primarily by renal excretion but its elimination has not been studied in anephric patients or in those with poorly functioning kidneys. It is not known [^{111}In-DTPA^{0}-D-Phe^{1}]-Octreotide can be removed by dialysis. Dosage adjustments in patients with decreased renal function have not been studied [25, 77].

Small peptides and protein fragments of appropriate charge and size (MW < 70 kDa) are initially filtered through the glomeruli and then get reabsorbed in the proximal tubules. The non-specific receptor system of megalin/cubulin (Fig. 4.15) contributes most to their reabsorption, through receptor-mediated endocytosis. Megalin and cubulin are multiligand, structurally dissimilar endocytic receptors (megalin is a transmembrane protein, while cubulin is not) located at the apical membrane of the proximal tubular cells and they operate in a synergistic fashion (Fig. 4.15). Studies in megalin-deficient mice revealed that the [^{111}In-DTPA^{0}-D-Phe^{1}]-Octreotide renal uptake was only 15–30% of that in the control mice [28, 56, 89–91].

After lysosome processing of the endocytosed [^{111}In-DTPA^{0}-D-Phe^{1}]-Octreotide, the trapped polar In-111 labeled degradation products in the proximal tubular cells burden the radiosensitive kidneys with unwanted radiation load (kidneys are the dose-limiting organs in PRRT). The renal uptake of [^{111}In-DTPA^{0}-D-Phe^{1}]-Octreotide appears to be facilitated by the electrostatic interaction between the slightly positive net charge of the molecule at a pH range 5–7, which is the usual pH range of the glomerular filtrate and the negatively charged proximal tubular cell surface. In Fig. 4.16, the electrophoretic mobility data on cellulose acetate (CAE: Cellulose Acetate Electrophoresis) of three Octreotide-based peptides with different net charge and lipophilicity are shown [12, 38, 80, 89]. In a comparative study of the renal uptake and metabolism between [^{111}In-DTPA^{0}-D-Phe^{1}]-Octreotide and the modified [^{111}In-DTPA^{0}-Asp^{0}-D-Phe^{1}]-Octreotide and [^{111}In-DTPA^{0}-D-Phe^{-1}-Asp^{0}-D-Phe^{1}]-Octreotide, it was concluded that the insertion of a negatively

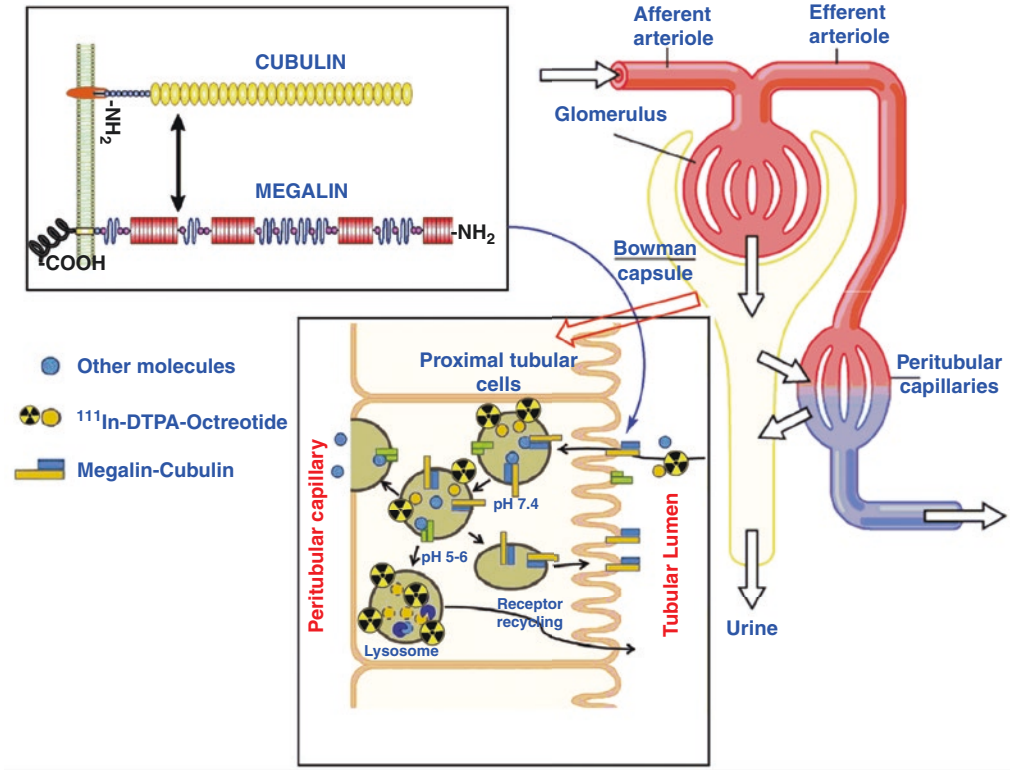

Fig. 4.15 Schematic depiction of the protein and peptide handling by the proximal tubular cells. The megalin/cubulin system located at the apex of the proximal tubular cells (nonselective system) mediates the reabsorption process for the [^{111}In-DTPA^{0}-D-Phe^{1}]-Octreotide, along with other molecules (i.e. albumin, vitamins, aminoacids). The acidic environment of the lysosomes leads to the trapping of labeled hydrolysis products of the [^{111}In-DTPA^{0}-D-Phe^{1}]-Octreotide molecule and contributes to the undesirable renal irradiation

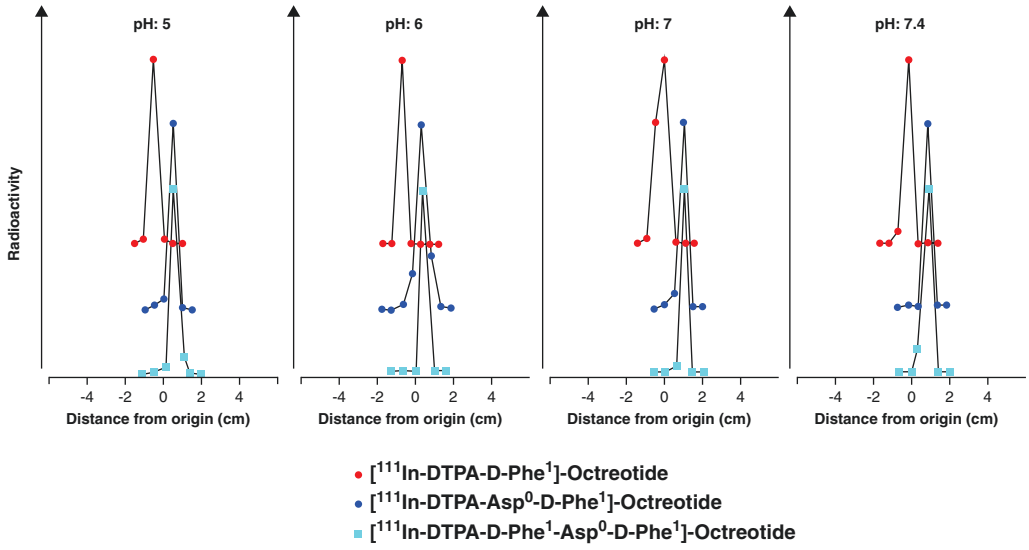

Fig. 4.16 The cellulose acetate electrophoresis (CAE) behavior of three structurally related peptides, at four different pH solutions, simulating urine and blood. The peptides differ in their net charge and lipophilicity [27, 89]

charged aspartic acid at the aminic end of the Octreotide molecule decreases its renal uptake due to the developing electrostatic repulsion, as it approaches the negatively charged proximal tubular cells. This result was further supported by the data of Akizawa et al. [27, 89].

4.8 Concluding Remarks

[^{111}In-DTPA^{0}-D-Phe^{1}]-Octreotide is a theragnostic radiopharmaceutical, which permits molecular imaging (SPECT or SPECT/CT) studies for acquisition of useful pre-therapy data (biodistribution, dosimetry, critical organ or tissue and the maximum tolerated dose), despite the limitations of In-111 as an Auger-emitting radionuclide. [^{111}In-DTPA^{0}-D-Phe^{1}]-Octreotide has been in use for more than two decades, mainly as an imaging agent and the experience that has been acquired formed the basis for the reevaluation of Auger emitters as radiotherapeutic agents. Indeed, extensive studies have proved that the small volume micrometastases of SSTR-expressing tumors can be successfully contained and possibly circulating tumor cells as well. Based on the findings of imaging results, dose ranging experiments, for higher dose-targeted molecular therapy and increased effectiveness, are thus allowed. All these factors lead to a tailored imaging and therapy approach to the same patient with [^{111}In-DTPA^{0}-D-Phe^{1}]-Octreotide as the modern personalized medicine approach dictates [80].

However, there is always ample room for improvement. Increasing the % uptake of the somatostatin analogue was an important step in this process, after the introduction of [DOTA^{0}-D-Phe^{1}-Tyr^{3}]-Octreotate (in which the C-terminal threoninol is replaced with threonine) by Kwekkeboom et al [88], which exhibited a nine-fold increased affinity for the $SSTR_2$ expressed by tumor cells compared with the affinity of [DOTA^{0}-D-Phe^{1}-Tyr^{3}]-Octreotide. The dimerization of the octreotide peptide ligand has been conclusively shown to increase the SSTR binding affinity with reduced background, opening the door to another possibility for improving the behavior of this class of ligands in the tumor radiotherapy setting [92]. Furthermore, experimental results with modifications in the incubation buffer used for the preparation of the In-111-labeled Octreotide analogue, which results in increased specific activity of the administered radiopharmaceutical and also the attachment of a nuclear localization sequence (NLS: Nuclear Localization Sequence) on the Octreotide molecule, are expected to augment the anti-tumor efficacy of these analogues, by maximizing the energy deposition of the Auger electrons in the region of the cell nucleus [3, 41, 93–97]. In addition, pharmacologic intervention for the sensitization of the replicating tumor cells, by interfering with the repair mechanisms of the DNA damage, is another clever strategy to increase therapeutic efficacy of the Auger-emitting radioligands. This approach has been attempted with Olaparib, a poly-[ADP-ribose]-polymerase 1 (PARP-1) inhibitor, which augments the cytotoxicity of the administered dose of the In-111-labeled preparation, by increasing the number of cytotoxic DSBs [98]. And lastly, the charge-modification of the NH_2-terminal-labeled somatostatin analogues, with the insertion of a negatively charged aspartic acid moiety therein, by facilitating its kidney excretion and reducing significantly the unwanted and deleterious kidney irradiation, allows the increase of the total administered Auger-emitter dose for higher therapeutic efficacy [27, 46].

References

1. Brazeau P, Vale W, Burgus R, et al. Hypothalamic polypeptide that inhibits the secretion of imunoreactive pituitary growth hormone. Science. 1973;179:77–9.
2. Weckbecker G, Lewis I, Albert R, et al. Opportunities in somatostatin research: biological, chemical and therapeutic aspects. Nat Rev Drug Discov. 2003;2:999–1017. https://doi.org/10.1038/nrd1255.
3. Bushberg JT, Seibert JA, Leid EM. The essential physics of medical imaging. 2nd ed. Philadelphia: Lippincott Williams & Wilkins; 2002.
4. De Lecea L, Criado JR, Prospero-Garcia O, et al. A cortical neuropeptide with neuronal depressant and sleep-modulating properties. Nature. 1996;381:242–5.
5. Gottero C, Prodam F, Destefanis S, et al. Cortistatin-17 and -14 exert the same endocrine activities

as somatostatin in humans. Growth Hormon IGF Res. 2004;14:382–7.
6. IUPAC-IUB Common Biochem Nomenclature. An one-letter notation for amino acid sequences. Tentative rules. Biochemistry. 1968;7:2703–5. https://doi.org/10.1021/bi00848a001.
7. Elliott DE. Somatostatin. 2001. https://epdf.tips/somatostatin9b1681210755ce0bffeb-5c27a17209b838154.html. Accessed 19 Oct 2018.
8. Bronstein-Sitton N. Somatostatin and the somatostatin receptors: versatile regulators of biological activity. 2018. https://www.alomone.com/article/somatostatin-somatostatin-receptors-versatile-regulators-biological-activity. Accessed 15 Oct 2018.
9. Barbieri F, Bajetto A, Pattarozzi A, et al. Peptide receptor targeting in cancer: the somatostatin paradigm. Int J Pept. 2013;2013:926295, 20 p. https://doi.org/10.1155/2013/926295.
10. Körner M, Reubi JC. Somatostatin. In: Kastin A, editor. Handbook of biologically active peptides. 1st ed. USA: Elsevier; 2006. p. 435–43.
11. Patel YC. Somatostatin and its receptor family. Front Neuroendocrinol. 1999;20:157–98.
12. Dalm DU, de Jong M. Comparing the use of radiolabeled SSTR agonists and an SSTR antagonist in breast cancer: does the model choice influence the outcome*?* EJNMMI Radiopharm Chem. 2017;2:11. https://doi.org/10.1186/s41181-017-0030-z.
13. Tulipano G, Schulz S. Novel insights in somatostatin receptor physiology. Eur J Endocrinol. 2007;156:S3–S11. https://doi.org/10.1530/eje.1.02354.
14. Reubi JC, Waser B, Mäcke H, et al. Highly increased ^{125}I-JR11 antagonist binding in vitro reveals novel indications for sst2 targeting in human cancers. J Nucl Med. 2017;58:300–6. https://doi.org/10.2967/jnumed.116.177733.
15. Hubalewska-Dydejczyk A, Signore A, de Jong M, Dierckx RA, Buscombe J, van de Wiele C, editors. Somatostatin analogues: from research to clinical practice. Hoboken: Wiley; 2015.
16. Günther T, Tulipano G, Dournaud P, et al. International Union of Basic and Clinical Pharmacology. CV. Somatostatin receptors: structure, function, ligands, and new nomenclature. Pharmacol Rev. 2018;70:763–835. https://doi.org/10.1124/pr.117.015388.
17. Patel RC, Kumar U, Lamb DC, et al. Ligand binding to somatostatin receptors induces receptor-specific oligomer formation in live cells. Proc Natl Acad Sci U S A. 2002;99:3294–9. https://doi.org/10.1073/pnas.042705099.
18. Reubi JC, Schonbrunn A. Illuminating somatostatin analog action at neuroendocrine tumor receptors. Trends Pharmacol Sci. 2013;34:676–88. https://doi.org/10.1016/j.tips.2013.10.001.
19. Reubi JC, Waser B, Schaer J-C, et al. Somatostatin receptor sst_1-sst_5 expression in normal and neoplastic human tissues using receptor autoradiography with subtype-selective ligands. Eur J Nucl Med. 2001;28:836–46. https://doi.org/10.1007/s002590100541.
20. Csaba Z, Peineau S, Dournaud P. Molecular mechanisms of somatostatin receptor trafficking. J Mol Endocrinol. 2012;48:R1–R12.
21. Fani M, Nicolas GP, Wild D. Somatostatin receptor antagonists for imaging and therapy. J Nucl Med. 2017;58:61S–6S. https://doi.org/10.2967/jnumed.116.186783.
22. Hofland LJ, Lamberts SWJ. The pathophysiological consequences of somatostatin receptor internalization and resistance. Endocr Rev. 2003;24:28–47. https://doi.org/10.1210/er.2000-0001.
23. Zhang X, Kim K-M. Multifactorial regulation of G protein-coupled receptor endocytosis. Biomol Ther. 2017;25:26–43.
24. Hanyaloglu AC, von Zastrow M. Regulation of GPCRs by endocytic membrane trafficking and its potential implications. Annu Rev Pharmacol Toxicol. 2008;48:537–68. https://doi.org/10.1146/annurev.pharmtox.48.113006.
25. Breeman WA, de Jong M, Kwekkeboom DJ, et al. Somatostatin receptor-mediated imaging and therapy: basic science, current knowledge, limitations and future perspectives. Eur J Nucl Med. 2001;28:1421–9. https://doi.org/10.1007/s002590100502.
26. Fani M, Braun F, Waser B, et al. Unexpected sensitivity of sst2 antagonists to N-terminal radiometal modifications. J Nucl Med. 2012;53:1481–9. https://doi.org/10.2967/jnumed.112.102764.
27. Oshima N, Akizawa H, Kawashima H, et al. Redesign of negatively charged ^{111}In-DTPA-octreotide derivative to reduce renal radioactivity. Nucl Med Biol. 2017;48:16–25.
28. Melis M, Krenning EP, Bernard BF, et al. Localisation and mechanism of renal retention of radiolabelled somatostatin analogues. Eur J Nucl Med Mol Imaging. 2005;32:1136–43. https://doi.org/10.1007/s00259-005-1793-0.
29. Fani M, Del Pozzo L, Abiraj K, et al. PET of somatostatin receptor-positive tumors using ^{64}Cu- and ^{68}Ga-somatostatin antagonists: the chelate makes the difference. J Nucl Med. 2011;52:1110–8. https://doi.org/10.2967/jnumed.111.087999.
30. Ginj M, Zhang H, Waser B, et al. Radiolabeled somatostatin receptor antagonists are preferable to agonists for in vivo peptide receptor targeting of tumors. Proc Natl Acad Sci U S A. 2006;103:16436–41. https://doi.org/10.1073/pnas.0607761103.
31. Kassis AI. Therapeutic radionuclides: biophysical and radiobiologic principles. Semin Nucl Med. 2008;38:358–66. https://doi.org/10.1053/j.semnuclmed.2008.05.002.
32. Kassis AI, Adelstein SJ. Considerations in the selection of radionuclides for cancer therapy. In: Welch MJ, Revanly CS, editors. Handbook of radiopharmaceuticals: Wiley; 2005. p. 767–93. https://doi.org/10.1002/0470846380.ch27.

33. Howel RW. Auger processes in the 21st century. Int J Radiat Biol. 2008;84:959–75. https://doi.org/10.1080/09553000802395527.
34. Duparc OH. Pierre Auger-Lise Meitner: comparative contributions to the Auger effect. Int J Mat Res (formerly Z Metallkd). 2009;100:1162–6. https://doi.org/10.3139/146.110163.
35. Feinendegen LE. Biological damage from the Auger effect, possible benefits. Radiat Environ Biophys. 1975;12:85–99.
36. Howell RW. Radiation spectra for Auger-electron emitting radionuclides: report No. 2 of AAPM Nuclear Medicine Task Group No. 6. Med Phys. 1992;19:1371–83. https://doi.org/10.1118/1.596927.
37. Lee BQ, Kibédi T, Stuchbery AE, et al. Atomic radiations in the decay of medical radioisotopes: a physics perspective. Comput Math Methods Med. 2012;2012:651475, 14 p. https://doi.org/10.1155/2012/651475.
38. McMillan DD, Maeda J, Bell JJ, et al. Validation of ^{64}Cu-ATSM damaging DNA via high-LET Auger electron emission. J Radiat Res. 2015;56:784–91. https://doi.org/10.1093/jrr/rrv042.
39. Cornelissen B, Vallis KA. Targeting the nucleus: an overview of Auger-electron radionuclide therapy. Curr Drug Discov Technol. 2010;7:263–79. https://doi.org/10.2174/157016310793360657.
40. Falzone N, Cornelissen B, Vallis KA. Auger emitting radiopharmaceuticals for cancer therapy. In: Gómez-Tejedor G, Fuss M, editors. Radiation damage in biomolecular systems. Biological and medical physics, biomedical engineering. Dordrecht: Springer; 2012.
41. Piroozfar B, Raisali G, Alirezapour B, et al. The effect of ^{111}In radionuclide distance and Auger electron energy on direct induction of DNA double strand breaks: a Monte Carlo study using Geant4-toolkit. Int J Radiat Biol. 2018;94(4):385–93. https://doi.org/10.1080/09553002.2018.1440329.
42. Bin Othman M, Mitry NR, Lewington VJ, et al. Re-assessing gallium-67 as a therapeutic radionuclide. Nucl Med Biol. 2017;46:12–8. https://doi.org/10.1016/j.nucmedbio.2016.10.008.
43. Thisgaard H. Accelerator based production of Auger-electron-emitting isotopes for radionuclide therapy. Dissertation, Risø National Laboratory for Sustainable Energy, Technical University of Denmark. 2008.
44. Thisgaard H, Jensen M. Sb-119: a potent Auger emitter for targeted radionuclide therapy. Med Phys. 2008;35:3839–46. https://doi.org/10.1118/1.2963993.
45. Stepanek J, Larsson B, Weinreich R. Auger-electron spectra of radionuclides for therapy and diagnostics. Acta Oncol. 1996;35:863–8. https://doi.org/10.3109/02841869609104038.
46. Fisher DR, Shen S, Meredith RF. MIRD dose estimate report No. 20: radiation absorbed-dose estimates for ^{111}In- and ^{90}Y-ibritumomab tiuxetan. J Nucl Med. 2009;50:644–52. https://doi.org/10.2967/jnumed.108.057331.
47. Lahiri S, Maiti M, Ghosh K. Production and separation of ^{111}In: an important radionuclide in life sciences: a mini review. J Radioanal Nucl Chem. 2012;297:309–18. https://doi.org/10.1007/s10967-012-2344-3.
48. Schlyer DJ. Production of radionuclides in accelerators. In: Welch MJ, Redvanly CS, editors. Handbook of radiopharmaceuticals: radiochemistry and applications. Hoboken: Wiley; 2003. p. 1–71.
49. Kocher DC. Radioactive decay data tables. DOE/TIC-11026, 115. 1981.
50. Tuck DG. Critical survey of stability constants of complexes of indium. Pure Appl Chem. 1983;55:1477–528.
51. Anderson CJ, Welch MJ. Radiometal-labeled agents (non-technetium) for diagnostic imaging. Chem Rev. 1999;99:2219–34. https://doi.org/10.1021/cr980451q.
52. Dilworth JR, Pascu SI. The radiopharmaceutical chemistry of gallium (III) and indium (III) for SPECT imaging. In: Long N, Wong W-T, editors. The chemistry of molecular imaging. 1st ed: Wiley; 2015. p. 165–76. https://doi.org/10.2967/jnumed.110.075101.
53. Harrison RC. Indium chemistry in radiopharmaceutical development. In: Cox PH, Mather SJ, Sampson CB, Lazarus CR, editors. Progress in radiopharmacy. Leiden: Martinus Nijhoff Publishers; 1986. p. 173–96.
54. Liu S. The role of coordination chemistry in the development of target-specific radiopharmaceuticals. Chem Soc Rev. 2004;33:445–61. https://doi.org/10.1039/b309961j.
55. Martell AE, Hancock RD. Factors governing the formation of complexes with unidentate ligands in aqueous solution. Some general considerations. In: Metal complexes in aqueous solutions. Springer US; 1996. p. 15–61.
56. Vegt E, de Jong M, Wetzels JFM, et al. Renal toxicity of radiolabeled peptides and antibody fragments: mechanisms, impact on radionuclide therapy, and strategies for prevention. J Nucl Med. 2010;51:1049–58. https://doi.org/10.2967/jnumed.110.075101.
57. Deferm C, Onghena B, Hoogerstraete V, et al. Speciation of indium (III) chloro complexes in the solvent extraction process from chloride aqueous solutions to ionic liquids. Dalton Trans. 2017;46:4412–21. https://doi.org/10.1039/c7dt00618g.
58. Ferri D. Complex formation equilibriums between indium (III) and chloride ions. Acta Chem Scand. 1972;26:733–46.
59. Harris WR, Chen Y, Wein K. Equilibrium constants for the binding of indium (III) to human serum transferrin. Inorg Chem. 1994;33:4991–8.
60. Yeh SM, Meares CF, Goodwin DA. Decomposition rates of radiopharmaceutical indium chelates in serum. J Radioanal Chem. 1979;53:327–36. https://doi.org/10.1007/bf02517931.
61. Layne WW, Hnatowich DJ, Doherty PW, et al. Evaluation of the viability of In-111-labeled DTPA coupled to fibrinogen. J Nucl Med. 1982;23:627–30.
62. Hsieh W-Y, Liu S. Synthesis, characterization, and structures of indium In(DTPA-BA_2) and

yttrium Y(DTPA-BA_2)(CH_3OH) complexes (BA benzylamine): models for ^{111}In- and ^{90}Y-labeled DTPA-biomolecule conjugates. Inorg Chem. 2004;43:6006–14.
63. Narita H, Tanaka M, Shiwaku H, et al. Structural properties of the inner coordination sphere of indium chloride complexes in organic and aqueous solutions. Dalton Trans. 2014;43:1630–5. https://doi.org/10.1039/c3dt52474d.
64. Sun Y, Motekaitis RJ, Martell AE, et al. N,N′-bis(2-mercaptoethyl)ethylenediamine-N,N′-diacetic acid; an effective ligand for indium(III). Inorgan Chim Acta. 1995;228:77–9. https://doi.org/10.1016/0020-1693(94)04392-9.
65. Ivanova VY, Chevela VV, Bezryadin SG. Complex formation of indium (III) with citric acid in aqueous solution. Russ Chem Bull. 2015;64:1842–9. https://doi.org/10.1007/s11172-015-1082-4.
66. Silva AMN, Kong X, Parkin MC, et al. Iron (III) citrate speciation in aqueous solution. Dalton Trans. 2009;0:8616–25. https://doi.org/10.1039/b910970f.
67. Thompson LCA, Pacer R. The solubility of indium hydroxide in acidic and basic media at 25°C. J Inorg Nucl Chem. 1963;25:1041–4. https://doi.org/10.1016/0022-1902(63)80039-1.
68. Maloney TJ, Camp AE Jr. Purification of indium 111. US Patent 6,162,648, 19 Dec 2000. 2000.
69. Brom M, Joosten L, Oyen WJG, et al. Improved labelling of DTPA- and DOTA conjugated peptides and antibodies with ^{111}In in HEPES and MES buffer. EJNMMI Res. 2012;2:4. https://doi.org/10.1186/2191-219X-2-4.
70. Balon HR, Brown TLY, Goldsmith SJ, et al. The SNM practice guideline for somatostatin receptor scintigraphy 2.0. J Nucl Med Technol. 2011;39:317–24.
71. Limouris GS, Chatziioannou A, Kontogeorgakos D, et al. Selective hepatic arterial infusion of In-111-DTPA-Phe^1-octreotide in neuro-endocrine liver metastases. Eur J Nucl Med Mol Imaging. 2008;35:1827–37.
72. OctreoScan™ package insert, Petten, The Netherlands, Mallinckrodt Medical B.V. September 2017 (revision).
73. Bakker WH, Albert R, Bruns C, et al. [^{111}In-DTPA-D-Phe^1]-octreotide, a potential radiopharmaceutical for imaging of somatostatin receptor-positive tumors: synthesis, radiolabeling and *in vitro* validation. Life Sci. 1991;49:1583–91. https://doi.org/10.1016/0024-3205(91)90052-d.
74. Maecke HR, Riesen A, Ritter W. The molecular structure of indium-DTPA. J Nucl Med. 1989;30:1235–1.
75. Siddons CJ. Metal ion complexing properties of amide donating ligands. Dissertation, University of North Carolina at Wilmington. 2004.
76. Bavelaar BM, Lee BQ, Gill MR, et al. Subcellular targeting of theranostic radionuclides. Front Pharmacol. 2018;9:996. https://doi.org/10.3389/fphar.2018.00996.
77. Capello A, Krenning EP, Wout AP, et al. Peptide receptor radionuclide therapy in vitro using [^{111}In-DTPA^0]-octreotide. J Nucl Med. 2003;44:98–104.
78. Reubi JC. Peptide receptors as molecular targets for cancer diagnosis and therapy. Endocr Rev. 2003;24:389–427. https://doi.org/10.1210/er.2002-0007.
79. Reubi JC, Schär J-C, Waser B, et al. Affinity profiles for human somatostatin receptor subtypes SST_1–SST_5 of somatostatin radiotracers selected for scintigraphic and radiotherapeutic use. Eur J Nucl Med. 2000;27:273–82. https://doi.org/10.1007/s002590050034.
80. van Essen M, Sundin A, Krenning EP. Neuroendocrine tumours: the role of imaging for diagnosis and therapy. Nat Rev Endocrinol. 2014;10:102–14. https://doi.org/10.1038/nrendo.2013.246.
81. Mariani G, Bodei L, Adelstein SJ, et al. Emerging roles for radiometabolic therapy of tumors based on auger electron emission. J Nucl Med. 2000;41:1519–21.
82. Eckelman WC, Frank JA, Brechbiel M. Theory and practice of imaging saturable binding sites. Invest Radiol. 2002;37:101–6.
83. Gokce A, Nakamura RM, Tubis M, et al. Synthesis of indium-labeled antibody-chelate conjugates for radioassays. Int J Nucl Med Biol. 1982;9:85–95. https://doi.org/10.1016/0047-0740(82)90034-1.
84. Jonard P, Jamar F, Walrand S. Effect of peptide amount on biodistribution of Y-86-DOTA-Tyr^3-octreotide (SMT487). J Nucl Med. 2000;41:260 p.
85. Breeman DWAP, Kwekkeboom DJ, Kooij PPM, et al. Effect of dose and specific activity on tissue, distribution of indium-111-pentetreotide in rats. J Nucl Med. 1995;36:623–7.
86. Wout AP, Breeman D, Kwekkeboom J, et al. Effect of dose and specific activity on tissue, distribution of indium-111-pentetreotide in rats. J Nucl Med. 1995;36:623–7.
87. Lewis JS, Lewis MR, Cutler PD, et al. Radiotherapy and dosimetry of ^{64}Cu-TETA-Tyr^3-octreotate in a somatostatin receptor-positive, tumor-bearing rat model. Clin Cancer Res. 1999;11:3608–16. https://doi.org/10.1158/1078-0432.CCR-04-1084.
88. Kwekkeboom J, Bakker DH, Kooij WP, et al. [^{177}Lu-DOTA^0-Tyr^3]-octreotate: comparison with [^{111}In-DTPA^0]-octreotide in patients. Eur J Nucl Med. 2001;28:1319–25.
89. Akizawa H, Arano Y, Mifune M. Effect of molecular charges on renal uptake of ^{111}In-DTPA-conjugated peptides. Nucl Med Biol. 2001;28:761–8.
90. Christensen EI, Birn H. Megalin and cubilin: multifunctional endocytic receptors. Nat Rev Mol Cell Biol. 2002;3:258–67. https://doi.org/10.1038/nrm778.
91. De Jong M, Barone R, Krenning E, et al. Megalin is essential for renal proximal tubule reabsorption of [^{111}In-DTPA^0]-Octreotide. J Nucl Med. 2005;46:1696–700.

92. Dong C, Zhao H, Yang S, et al. ^{99m}Tc-labeled dimeric octreotide peptide: a radiotracer with high tumor uptake for single-photon emission computed tomography imaging of somatostatin receptor subtype 2-positive tumors. Mol Pharm. 2013;10:2925–33. https://doi.org/10.1021/mp400040z.
93. Chen P, Wang J, Hope K, et al. Nuclear localizing sequences promote nuclear translocation and enhance the radiotoxicity of the anti-CD33 monoclonal antibody HuM195 labeled with ^{111}In in human myeloid leukemia cells. J Nucl Med. 2006;47:827–36.
94. Ginj M, Hinni K, Tschumi S, et al. Trifunctional somatostatin-based derivatives designed for targeted radiotherapy using Auger electron emitters. J Nucl Med. 2005;46:2097–103.
95. Hillyar C. Auger electron radionuclide therapy utilizing F3 peptide to target the nucleolus. Dissertation, Jesus College, University of Oxford. 2015.
96. Cornelissen B, Able S, Kersemans V, et al. Nanographene oxide-based radioimmunoconstructs for in vivo targeting and SPECT imaging of HER2-positive tumors. Biomaterials. 2013;34:1146–54. https://doi.org/10.1016/j.biomaterials.2012.10.054.
97. Kersemans V, Kersemans K, Cornelissen B. Cell penetrating peptides for in vivo molecular imaging applications. Curr Pharm Des. 2008;14:2415–27. https://doi.org/10.2174/138161208785777432.
98. Nayak TK, Atcher RW, Prossnitz ER, et al. Enhancement of somatostatin-receptor-targeted ^{177}Lu-[DOTA^{0}-Tyr^{3}]-octreotide therapy by gemcitabine pretreatment-mediated receptor uptake, up-regulation and cell cycle modulation. Nucl Med Biol. 2008;35:673–8. https://doi.org/10.1016/j.nucmedbio.2008.05.003.